Available online at www.sciencedirect.com
SCIENCE DIRECT
Coordination Chemistry Reviews 250 (2006) 1294–1314
COORDINATION CHEMISTRY REVIEWS
www.elsevier.com/locate/ccr

Review

Recent trends on nanocomposites based on Cu, Ag and Au clusters: A closer look

Lidia Armelao [a], Davide Barreca [a], Gregorio Bottaro [a], Alberto Gasparotto [b], Silvia Gross [a], Cinzia Maragno [b], Eugenio Tondello [b,*]

[a] *ISTM-CNR and INSTM, Department of Chemistry, University of Padova, Via Marzolo, 1-35131 Padova, Italy*
[b] *Department of Chemistry, University of Padova and INSTM, Via Marzolo, 1-35131 Padova, Italy*

Received 27 July 2005; accepted 3 December 2005
Available online 10 January 2006

Contents

Abstract

Nanocomposite materials based on metal nanoparticles (NPs, *guest*) in/on oxide matrices (*host*) have attracted increasing attention thanks to their intriguing chemico-physical properties that can be tailored as a function of NP size, shape and mutual interactions. The possibility to obtain a controlled dispersion of metal particles in/on suitable oxides (*inside-* and *outside-cluster* systems, respectively) paves the way to a broad spectrum of technological applications, ranging from heterogeneous catalysis, to gas sensing and non-linear optics. The control of functional performances relies on tailoring the system properties by design through a suitable choice of the synthesis and processing routes.

In this context, the present review provides a synoptic overview on our recent research activity concerning nanocomposites containing 11th group metal clusters (Cu, Ag and Au), dispersed in/on oxide matrices (SiO_2, TiO_2, Al_2O_3). We begin by briefly outlining the interest and size-dependent properties of such systems. Subsequently, the attention is switched to a survey on the preparation strategies previously adopted in the literature,

Abbreviations: 0D, zero-dimensional; 1D, mono-dimensional; 2D, bi-dimensional; 3D, three-dimensional; α, Auger parameter; AAO, anodic aluminum oxide; AFM, atomic force microscopy; BE, binding energy; BF, bright field; CVD, chemical vapor deposition; DC, direct current; GIXRD, glancing incidence X-ray diffraction; EDS, energy dispersive X-ray spectroscopy; fcc, face-centered cubic; HR-TEM, high resolution-transmission electron microscopy; KE, kinetic energy; LRI, laser reflection interferometry; MDR, morphological dependent resonance; NPs, nanoparticles; NTs, nanotubes; p, total pressure applied to a plasma discharge; PE-CVD, plasma enhanced-chemical vapor deposition; R, reflectance; RF, radio-frequency; SAED, selected area electron diffraction; SEM, scanning electron microscopy; SERS, surface-enhanced Raman scattering; SG, sol–gel; SIMS, secondary ion mass spectrometry; SMMs, single-molecule magnets; SPR, surface plasmon resonance; t, deposition time; T, temperature; TEOS, tetraethoxysilane; V_{bias}, self-bias potential; W, RF-power applied to a plasma discharge; $\chi^{(3)}$, third-order non-linear susceptibility; XE-AES, X-ray excited auger electron spectroscopy; XPS, X-ray photoelectron spectroscopy

* Corresponding author. Tel.: +39 0498275220; fax: +39 0498275161.
E-mail address: eugenio.tondello@unipd.it (E. Tondello).

doi:10.1016/j.ccr.2005.12.003

focusing in particular on the use of *soft* methods, such as sol–gel (SG), RF-sputtering and their innovative combination. The most relevant results on M'/M_xO_y nanocomposites (where M′ = Cu, Ag, Au and M = Si, Ti, Al) obtained by these routes are then comparatively discussed, highlighting analogies and differences between them. Finally, the most attractive research perspectives in the field are briefly presented.

Keywords: Metal nanoparticles; Nanocomposites; Preparation techniques; Sol–gel; RF-sputtering

1. Introduction

The last decade has witnessed an exponential growth of research activities on composite materials based on metal NPs (*guest*) in/on suitable oxide matrices (*host*), thanks to the possibility of tailoring their chemico-physical properties as a function of particle size, shape and distribution [1–14]. This widespread scientific and technological interest has been mainly driven by the concurrence of two causes, namely the full understanding of nanocomposite behavior and the potential hope for functional applications and economic impact. As a matter of fact, the novel features acquired on the *nano*-dimensional regime are not a mere result of scaling factors [15], but rather stem from the confinement of charge carriers [16] and the enhancement of the surface-to-volume ratio on decreasing NPs dimensions [8,15,17,18], resulting in a spectrum of size-dependent properties widely diversified from the corresponding bulk counterparts [3,19–28]. Studies on this evolution might help to elucidate how properties depend on size in the regime between molecules and solid-state materials [19,29].

Unique characteristics are also derived from interfacial NP/matrix interactions, that might appreciably depend on the presence of defects, compositional gradients and roughness and play a pivotal role on the system functional performances [7,8,30–40]. Moreover, the chemical composition and surface structure of *guest* NPs might result unstable due to their high reactivity and energy content [16], leading thus to a progressive alteration of the system properties under prolonged use. As a consequence, a full exploitation of the nanosystem potential in advanced device structures relies on a thorough understanding of their stability and general properties, with particular regard to their structure, chemical composition and morphology.

In this context, materials based on clusters of 11th group metals (Cu, Ag, Au) have fascinated people for centuries, providing colors for the Medieval cathedral windows, as well as for vases, pottery and other ornaments [15,16,19,41–45]. Actually, these systems stimulate considerable interest in various research fields, due to their intriguing chemico-physical characteristics and their potential application in catalysis, microelectronics, sensing, magnetism, photonics and energetics [12,16,25,46]. More specific examples include labels for biomolecules, bio- and gas sensors, ultrafast optical switches, optical filters and tweezers [8,11,19,20,26,47–49]. In particular, as metal particles are reduced in size to tenths of nanometers, a dramatic change in their optical properties occurs, resulting from the collective oscillation of electrons in the conduction band [50]. This phenomenon, the so-called SPR, leads to a characteristic absorption of the visible light [16,43,47]. The frequency and intensity of the SPR signal are typical of the type of *host–guest* materials [50] and are highly sensitive to the size, size distribution and shape of the NPs [51], as well as to the nature of the surrounding medium [52]. This direct correspondence between NP features and their optical response, resulting in the so-called MDRs [53], has prompted the ongoing intense interest in the optical properties of Cu, Ag and Au clusters dispersed in/on various media, fueling the construction of SPR-based sensors and devices in ever increasing variety.

Among the various supporting/embedding *hosts* for such metal NPs, metal oxides have received a significant attention [54], owing to their different structures and chemico-physical characteristics. In particular, oxide matrices such as SiO_2, TiO_2 and Al_2O_3 have been thoroughly investigated thanks to their amenable features, such as optical transparency in the visible range, insulating character, structural and thermal stability and weak interactions with *guest* particles [11,30,31,55–58].

Host–guest systems containing gold and silver NPs have been the subject of several investigations such as heterogeneous catalysis [4,5,20,35,36,38,48,59–68], gas sensing [6,35,49,69,70], as well as optics and optoelectronics [2,5,14,57,61,71–79], thanks to the peculiar properties arising when their size is comparable or lower than the electron mean free path [16,18,80–83]. Specific examples in these fields concern SERS experiments, where such NPs are frequently used for signal enhancement [26,46,51,84,85]. Au- and Ag-based nanocomposites have also been employed in a variety of catalytic processes such as CO oxidation, NO_x reduction and water gas shift reaction [13,20,21,33,36,48,70,86–92]. Furthermore, oxide-based materials containing Cu, Ag and Au nanoclusters are attractive candidates for the design and development of integrated all-optical devices with controllable non-linear properties [2,27,74,75,83,93–100], thanks to their fast response times and large third-order non-linear susceptibility ($\chi^{(3)}$) values, that are strongly enhanced near the SPR frequency [74–79,81,94,96,101–106].

Beyond non-linear optical devices, Au/TiO_2 have been increasingly employed in photoelectrochemical solar cells, thanks to the well-known photocatalytic properties of TiO_2 [107,108] that are further enhanced by gold dispersion [109]. Dye-sensitized nanocrystalline TiO_2 solar cells have achieved sunlight-to-electrical power conversion efficiencies greater than 9% and photocurrents >16 mA cm^{-2} [110].

In this review, we present the synthesis and properties of oxide-based nanocomposites containing 11th group NPs, focusing on the most relevant results obtained by our research team in the last years [53,111–118]. A schematic representation of the nanocomposites that are the subject of the present work is

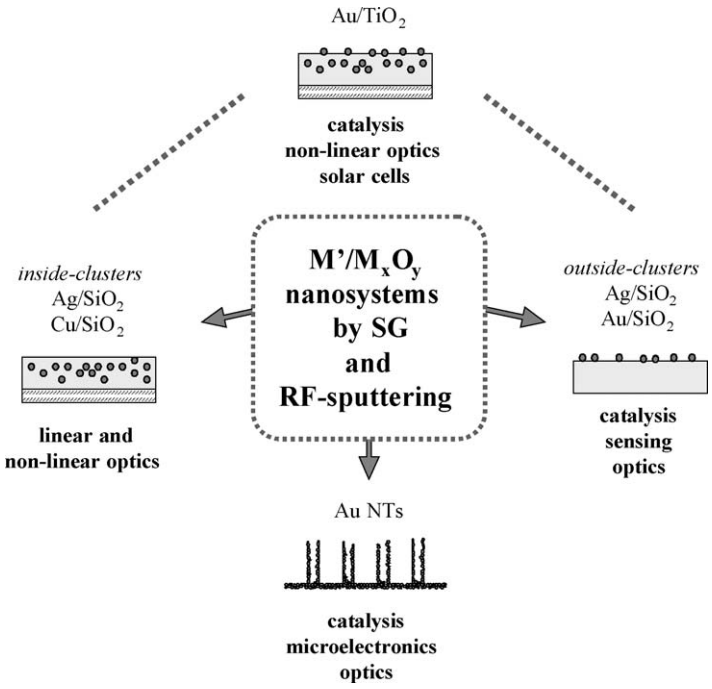

Fig. 1. Sketch of the different categories of M'/M_xO_y nanosystems considered in the present review and related technological applications.

proposed in Fig. 1. The major difference between *inside-cluster* (Section 3, Ag/SiO_2 and Cu/SiO_2) and *outside-cluster* systems (Section 4, Ag/SiO_2 and Au/SiO_2) is represented by the spatial distribution of *guest* metal NPs in the *host* matrix. While in the first case, the aggregates are dispersed *inside* the SiO_2 *host* that also serves as a protective medium for them, in the latter case they are distributed only on the silica surface. Au/TiO_2 nanocomposites are mid-way between these two groups, gold NPs being present both on the surface and sub-surface titania layers. Obviously, the technological applications and intrinsic features of these systems are different. Whereas *inside-cluster* composites are mainly interesting for optical devices, *outside-cluster* ones are also of relevance in the field of heterogeneous catalysis and sensing.

A further system modulation can be achieved by the *controlled assembly* of metal nanoparticles into more complex shaped structures [16,119]. In a similar philosophy, NPs are regarded as small "building blocks" that are hierarchically organized in super-structures by means of suitable preparation routes [19]. Among the various kinds of NPs-based architectures, specific examples are represented by 0D, 1D and 2D nanosystems including, for instance, quantum-dots, nanowires/nanotubes and 2D arrays [119–121]. To this regard, other fascinating systems, briefly discussed in the final part of this review, are represented by metal NPs dispersed in the pores of oxide membranes provided with 1D channels, resulting in the formation of Au NTs (Fig. 1). These mono-dimensional metal arrays are promising candidates in many research fields thanks to their anisotropic properties [121–123], that can be exploited in several advanced applications, such as microelectronic devices, sensors with improved performances [123–126], alignment features in liquid crystal displays [127], novel heterogeneous catalysts [128], magnetic storage media with high capacities [129,130], field-emission displays and optical energy transport systems [131].

Specifically, among the various metals, gold-based 1D nanosystems are attractive elements in device structures for their low resistivity and chemical stability, as well as in thiol-based bio-sensors in DNA chips [132] and advanced optical systems [123].

The present contribution starts with a brief introduction on the different preparation routes proposed in the literature for the synthesis of Cu-, Ag- and Au-containing nanocomposites. Due to the huge number of scientific publications in this field, this work is far from providing an exhaustive review on the previously performed research activities. Our aim is rather to present a survey of the more significant results obtained in the *bottom-up* synthesis of nanocomposites, focusing in particular on SG, RF-sputtering and their innovative combination. For a more detailed discussion on these methodologies, the reader can refer to specific pertinent literature.

In particular, we will comparatively report the most relevant features pertaining to the synthesis and tailoring of M'/M_xO_y nanocomposites ($M' = Cu, Ag, Au$; $M_xO_y = SiO_2, TiO_2, Al_2O_3$), focusing on their structure, composition, morphology, optical properties and their mutual interrelations with the processing parameters. Emphasis will be given to the possibility of obtaining prescribed nanosystem properties by a proper choice of the synthesis and treatment conditions. The nanocomposite peculiarities arising from the NPs distribution and/or reactivity with the surrounding medium, also depending on the nanometric particle size, are outlined and discussed.

2. Preparation strategies for nanocomposites based on metal clusters: the role of sol–gel, RF-sputtering and hybrid RF-sputtering/sol–gel routes

An open challenge in the field of nanotechnology is the development of versatile synthetic strategies to control the nucleation of the material building blocks and their subsequent assembly on the nanometric scale into ordered 0D-, 1D-, 2D- and 3D-structures [15,119,123,133,134]. As a matter of fact, tailoring of nucleation/growth processes is a key step to improve specific system characteristics, thus allowing the design of new and more efficient functional devices provided with optimized performances [13,14,135].

In the particular context of embedded and supported metal NPs, much research work has been focused on exploring both solution- and vapor-phase approaches, as well as on the influence of the matrix surface in directing the nano-unit nucleation and subsequent organization [136].

Up to date, M'/M_xO_y-based nanocomposites have been synthesized by several chemical and physical routes, including CVD [70,137], SG and impregnation [8,14,35,36,57,89,97,118,138–153], wet chemical methods and layer-by-layer self-assembly [8,13,20,27,71,77,93,154–160], ion beam-assisted techniques [11,55,56,103,161,162], ion implantation [55,76,163–165], combined thermal and electron beam deposition [166], evaporation [4,33,34,92,167–171], sputtering

[2,40,53,73,75,79,94–96,101,102,105,113,116,172–180] and joint sputtering/PE-CVD [181].

An attractive *bottom-up* preparation strategy for the synthesis of M'/M_xO_y nanocomposites is the SG process [182–184], a versatile low-temperature approach from the liquid to the solid-state [57,118,142,143,185–194]. The system assembly is obtained starting from a suitable precursor solution through hydrolysis and condensation reactions, that lead to the formation of oxo-based macromolecular networks, providing the unique possibility of tailoring the system evolution according to the desired process path. To this regard, the first steps of the SG reactions, involving the formation of inorganic building blocks, are particularly critical. In fact, several parameters including precursor nature and concentration, solvent nature, hydrolysis ratio, presence and nature of catalysts, pH, as well as aging time and temperature [195], influence not only the network type (polymer or cluster-like), but also the cross-linking density [196]. The modulation of these factors enables one to achieve variations in the structure and properties of SG-derived networks over a wide range [197]. These peculiarities, together with the mild synthesis conditions (*soft chemistry*), make the SG method particularly suitable for yielding thin films and composites with good control over NPs size, size distribution, structure and concentration.

As regards nanocomposites based on metal NPs, the SG route is particularly versatile in the preparation of *inside-clusters* with controlled dispersion in the *host* oxide (Fig. 1). Since the nanosized particles are formed inside a highly viscous matrix, their growth and size distribution can be controlled and tailored. Interestingly, the formation of the *host* and *guest* phases in the final system can be performed by a *single-step* process thanks to the molecular-level mixing of reactants in the starting solutions. Alternatively, processing with suitable functionalized precursors (for instance, organofunctional alkoxysilanes of the type $R'Si(OR)_3$, with R = alkyl group and R′ = amino-, thiourea-, thiolate- or acetylacetonate moieties) [186,190,192,198–200] can play a significant role in promoting a *chemical anchoring* of metal species to the forming oxide *host* matrix, avoiding undesired aggregation phenomena [201] and enabling a fine control of NPs dispersion. In the present review, both kind of approaches will be demonstrated in two specific case studies concerning the preparation of Ag/SiO_2 and Cu/SiO_2 nanocomposites, as outlined in Section 3.

Among the various vapor-phase synthetic routes to M'/M_xO_y *outside-cluster* systems, RF-sputtering is one of the most feasible thanks to its inherent versatility and the capability of obtaining an homogeneous surface coverage at low temperatures under controlled processing conditions [83]. Basically, the process involves the ablation of a metal target by a weakly ionized plasma (ignited by the use of a fixed-frequency RF discharge) and the condensation of the ejected metal species on a suitable substrate [202] (in the present case, an oxide matrix). During sputtering, the deposited particles undergo nucleation and growth phenomena, resulting in the formation of nanosystems with peculiar morphology as a function of the adopted preparative conditions. Key advantages of the RF-sputtering process over other preparation routes are the possibility of controlling the metal content up to high concentrations [74,75], the potential to fabricate materials with very high melting points, which are hardly obtainable by evaporation [176], the flexibility that permits the preparation of composite films of various metals and dielectric materials and the capability to produce metal NPs with controlled size, shape and distribution [74,203] by exploiting the ubiquitous competition between ablation and deposition processes characterizing non-equilibrium glow discharges [53]. The modulation of the material features arises from a proper choice of process parameters (RF-power, operating pressure, substrate temperature, deposition time), that have a combined influence on both homogeneous and heterogeneous processes occurring in the plasma, and hence, on the chemical and physical properties of the final system (Section 4).

A step beyond in the advance of synthetic strategies for composites containing metal NPs is represented by the synergic combination of RF-sputtering and SG routes, resulting in innovative hybrid approaches [111]. In particular, based on our recent studies concerning similar CVD/SG joint strategies [204–208], the attention here is focused on the dispersion of metal NPs by RF-sputtering into porous as-prepared SG matrices (xerogels) and on subsequent thermal treatments of the obtained composite systems (Fig. 2). Such a hybrid RF-sputtering/SG route to metal NPs-containing nanocomposites has been adopted in the present work for the tailored synthesis of Au/TiO_2 nanosystems (Section 5) [111]. To the best of our knowledge, only a few reports concerning the preparation of nanocomposites containing metal NPs by hybrid liquid/vapor-phase routes have, so far, appeared in the literature [209,210].

The use of a xerogel layer as a substrate enables to explore variations of the chemico-physical properties under thermal evolution, with particular regard to the in-depth distribution and dispersion of the *guest* NPs in the *host* matrix and their mutual interactions. As a matter of fact, xerogels, characterized by the presence of non-bridging bonds, provide reaction sites for successive chemical modifications both on the surface and sub-surface layers [111,204,205], enabling, in principle, an optimal dispersion of the deposited metal NPs. Moreover, xerogels are particularly suitable as *hosts* thanks to their inherent porous structure, that can be exploited to achieve NP confinement and quantum-dot growth [211]. A further aspect of crucial importance in order to obtain NPs with tailored size and distribution is the competition between deposition/ablation phenomena characterizing sputtering processes from glow discharges [53]. Moreover, plasma activation of both gas-phase species and growth surface can promote intermixing processes between the *host* matrix and the *guest* phase already in the as-prepared systems. The synergic combination of these features might result in unexpected and/or improved functional properties. In the present case, due to the *soft* conditions adopted for RF-sputtering experiments, plasma-assisted chemico-physical modifications of the xerogel are expected to involve essentially the outermost sample region. Finally, ex situ thermal treatments could induce either a coalescence of the metal particles in the near-surface region or their migration in the inner layers of the *host* matrix, depending on the experimental parameters [111]. To this regard, representative examples will be shown in detail in Section 5.

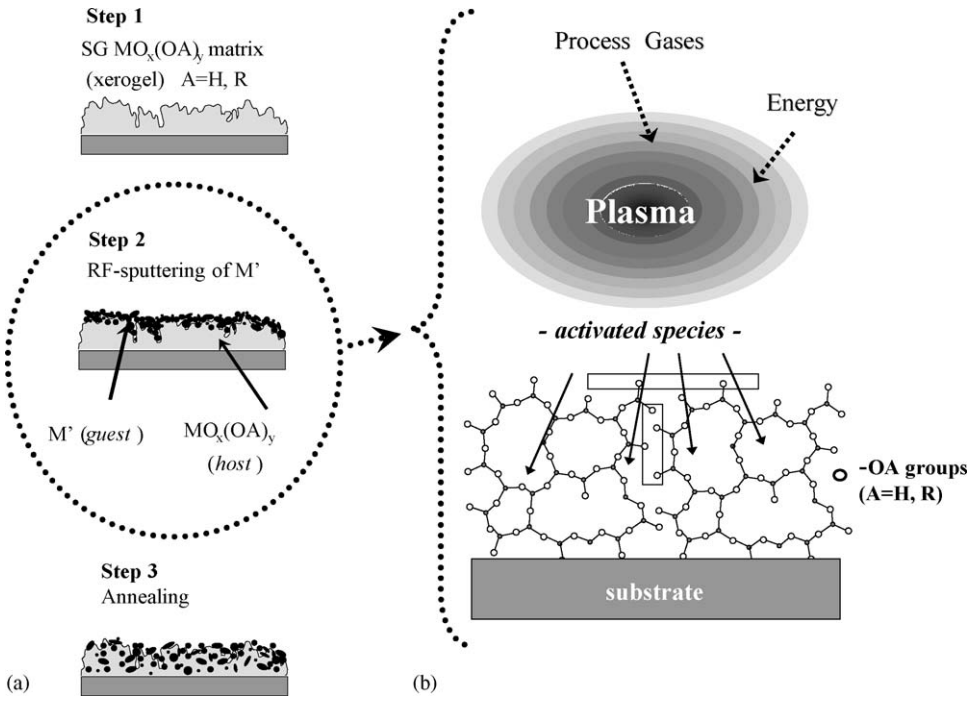

Fig. 2. (a) Schematic representation of the hybrid RF-sputtering/SG synthetic approach. (b) More detailed sketch of step 2. The −OA groups (A = H, R) are demonstrated in the boxes (adapted from [205]).

3. *Inside-cluster* systems: Ag/SiO_2 and Cu/SiO_2 by sol–gel

The present section is devoted to the presentation of relevant results for the SG synthesis of silica coatings doped with silver [118,212] and copper NPs [117,213]. The as-prepared samples only contain the Ag(I) and Cu(II) cations, which can evolve to metallic particles after suitable ex situ thermal treatments. In this regard, whereas in the synthesis of Ag–silica *host–guest* composites metallic silver clusters are easily obtained, an important issue for the analogous copper-containing systems is represented by the variety of possible oxidation states for copper in the *guest* nanoparticles. In fact, copper forms two stable semiconducting oxides, *tenorite* (CuO) and *cuprite* (Cu_2O), and both have been prepared as embedded NPs in silica glasses by various chemical and physical methods [214–218]. Conversely, the formation of *single-phase* metallic Cu NPs in silica is not straightforward and has to be pursued by a proper combination of synthesis parameters and processing conditions (annealing temperature, time and atmosphere). As a consequence, beyond the control of NP size and distribution, the tailoring of the *guest* copper-phase composition in the *host* silica matrix constitutes a major concern.

To our knowledge, whereas many studies have appeared in literature on the SG growth of Ag crystallites in/on various oxide-based matrices (compare Section 2), there are only few available reports on the formation of copper-based nanosystems up to date [97,139,140,142–151].

For both Ag/SiO_2 and Cu/SiO_2 nanocomposites described in the following paragraphs, SG films were obtained on amorphous silica slides by the dip-coating procedure, performed in air at room temperature [117,118,212,213].

3.1. Ag/SiO_2 nanosystems

In this paragraph, we discuss some selected experimental results concerning Ag/SiO_2 *inside-cluster* systems obtained by the SG technique, exploiting the peculiar advantages of this route outlined in the previous section.

In the SG synthesis of metal-doped silica coatings, two main aspects have to be taken into account, namely the control of film composition and of NPs size and distribution. To prevent the uncontrolled formation of metal particles in the starting solution, the amino-functionalized silane *N*-[3-(trimethoxysilyl)propyl]-ethylenediamine $[(CH_3O)_3Si(CH_2)_3NH(CH_2)_2NH_2]$ [219,220] and silver acetate were used as precursors for the silica network and the metallic phase, respectively. As a matter of fact, the use of a precursor in which the silane moiety originating the silica *host* matrix is combined with amino-groups able to "anchor" the silver ions, allows the simultaneous formation of the *host* network and of the *guest* nanoparticles, enabling at the same time an effective control over the particle size and distribution.

SG solutions of the precursors were prepared in isopropyl alcohol, also adding controlled amounts of H_2O and CH_3COOH, so that hydrolysis occurred under acid conditions [118,212]. Ex situ thermal treatments in air were performed at temperatures between 400 and 800 °C for 1 h, in order to investigate the thermal evolution of the as-prepared samples.

After annealing in air for 1 h at 600 °C, the precursor decomposition was complete: in this case silver NPs were well separated and homogeneously dispersed inside a very pure *host* silica matrix, as pointed out by TEM analyses (Fig. 3). In particular, two cluster populations with different sizes (≈2 and ≈7 nm, respectively) were observed. Interestingly, HR-TEM analysis

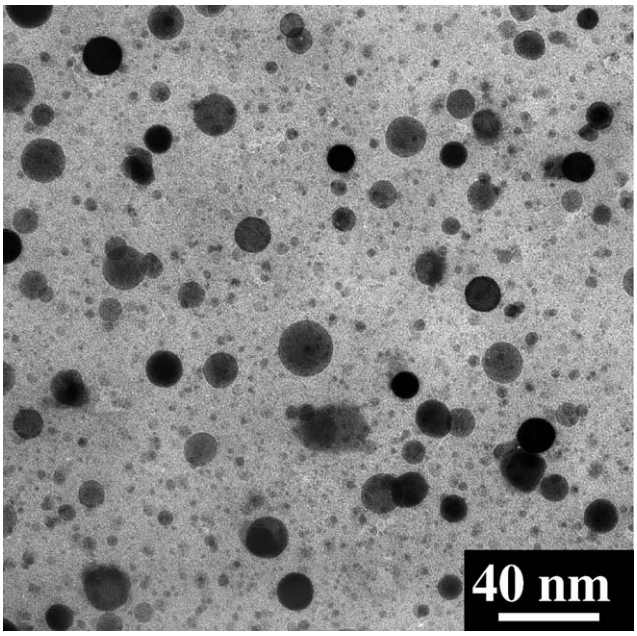

Fig. 3. BF-TEM plane-view micrograph for an Ag/SiO_2 specimen annealed in air at 600 °C for 1 h (adapted from [118,212]).

indicated that some of the particles were not spherical, but rather exhibited a faceted shape (Fig. 4). Concerning the NPs chemical composition, XPS and XE-AES showed that the silver oxidation state changed with temperature. In particular, the analysis aimed at determining the co-presence of Ag(0) and Ag(I) required great attention. Since the XPS peak positions of these two species are comparable [114,118,221,222], the calculation of the Auger parameters α_1 [BE($Ag3d_{5/2}$) + KE(AgM_5NN)] and α_2 [BE($Ag3d_{5/2}$) + KE(AgM_4NN)] was necessary to solve the question [223,224]. In particular, at temperatures up to 550 °C silver was still partly oxidized [Ag(I)], while in the 600 °C-heated sample almost all the silver was in the metallic state. Nevertheless, a faint interaction between silver nanoclusters and the surrounding silica matrix was pointed out by SIMS analysis. Such investigation showed both AgO^+ and $AgOSi^+$ fragments, ascribed to the presence of some oxidized silver atoms and to the formation of a silicate *shell* surrounding the NPs [118]. The formation of crystalline Ag in the samples was not detected up to an annealing temperature of 600 °C, at which sharp diffraction peaks ascribable to fcc metal silver were instead observed. Moreover, optical absorption spectrum of the sample heated at 600 °C was characterized by a very intense and narrow band, peaked at $\lambda = 407$ nm (Fig. 5) and ascribed to the SPR of silver NPs in silica. For higher annealing temperatures (800 °C), the oxidation state of silver atoms changed abruptly, since Ag(0) atoms underwent a complete oxidation to Ag(I).

A realistic hypothesis explaining the Ag NPs formation and the consequent color change of the coatings is based on a temperature-dependent redox mechanism [118]. XPS investigation showed that at temperatures up to 550 °C Ag(I) ions were progressively reduced to Ag(0) by the amino-groups present in the silane precursor, which were, in turn, oxidized. This reaction and the consequent aggregation of Ag(0) species to form silver clusters induced a color change of the coatings from transparent to pale yellow. At 600 °C metallic NPs, producing an intense yellow coloration, were present in the films, as proved by both XRD and TEM analyses. Again, systems heated in air at $T \geq 800$ °C

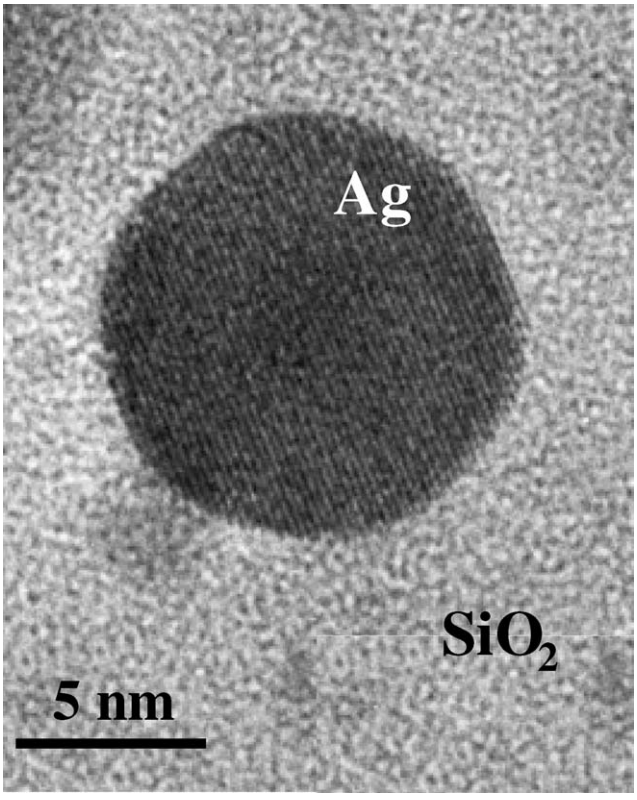

Fig. 4. HR-TEM micrograph of an Ag/SiO_2 layer annealed in air at 600 °C for 1 h. The icosahedric shape of the silver nanoparticle is clearly visible, as well as the lattice fringes of (1 1 1) silver planes (adapted from [212]).

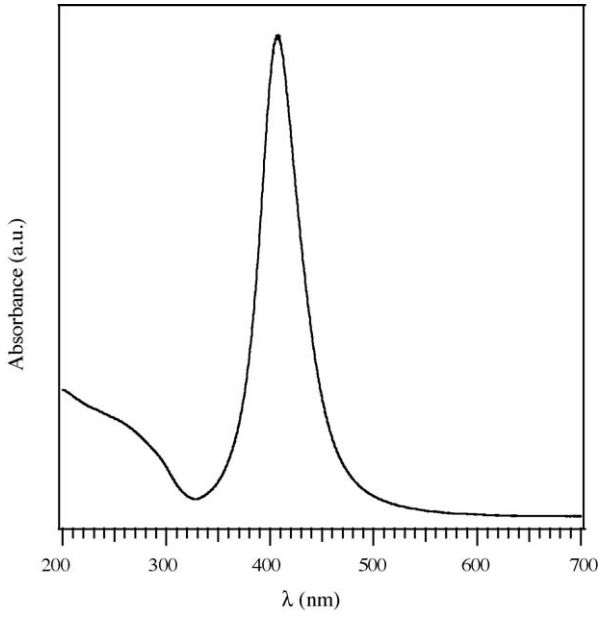

Fig. 5. Optical absorption spectrum of an Ag/SiO_2 nanocomposite annealed in air at 600 °C for 1 h (adapted from [118]).

appeared completely colorless due to the Ag(0) → Ag(I) conversion.

In summary, the tailoring of size, distribution and stability of Ag NPs in SiO_2 has been obtained on the basis of the proper choice of SG processing conditions, combined with a careful thermal treatment. The tunable composition and structure of the resulting composites are of great interest, since most of their advanced technological applications require an accurate control of these features.

3.2. *Cu/SiO_2 nanosystems*

In the previous paragraph, we have outlined the main features of Ag/SiO_2 nanocomposites, obtained by SG starting from suitably functionalized precursor compounds. A valuable alternative to obtain M'/M_xO_y systems via SG exploits the molecular-level mixing of reactants in the starting solutions. The feasibility of such a strategy will be demonstrated in the present paragraph, focused on the design and synthesis of Cu/SiO_2 nanosystems.

Composite silica coatings containing copper NPs were prepared from ethanolic solutions of TEOS and Cu(II) acetate. In analogy to silver–silica nanosystems, the as-prepared samples only contained Cu(II) cations, which evolved to *tenorite* (CuO), *cuprite* (Cu_2O) or metallic Cu crystallites depending on thermal treatment conditions: temperature (100–900 °C), time (1–5 h) and atmosphere (air, N_2, 4% H_2 in N_2) [117]. In all samples, a homogenous distribution of copper-containing NPs in the SG silica matrix was observed, as demonstrated by TEM analysis (Fig. 6). The crystalline phase first obtained by treatments under both air and nitrogen atmospheres was *tenorite*. Whereas it was stable in air over a wide temperature range (up to 900 °C), prolonged treatments under flowing N_2 (up to 5 h) resulted in the formation of *cuprite*, due to the low stability of CuO in oxygen-deficient atmospheres [225,226]. Consequently, the formation of crystalline clusters containing reduced copper species was studied by treating the as-prepared samples in H_2 (4% in N_2). The effect of H_2–N_2 atmosphere on the system composition and microstructure was well demonstrated after heating at 900 °C. Higher treatment temperatures were not adopted to avoid undesired reactions between the *guest* species and the *host* silica matrix. In these conditions, a prolonged annealing (up to 5 h) resulted in the progressive appearance of crystalline Cu at expenses of the CuO crystal phase, even if *tenorite* was still present in the sample. In fact, as shown in the GIXRD spectra of Fig. 7, *tenorite* peaks were accompanied by the typical reflections of fcc metallic copper. The Cu(II) → Cu(0) reduction process in samples treated under H_2–N_2 flow was also investigated by UV–visible analysis (Fig. 8). As can be observed, prolonged annealing at 900 °C favored a progressive cupric-to-metallic copper conversion, as confirmed by the intensity increase of the Cu NPs SPR band located at $\lambda \approx 570$ nm [50,214]. However, in order to attain a complete transformation of Cu(II) species into Cu ones, an alternative route was followed. Previously N_2-treated (900 °C, 5 h) Cu_2O/SiO_2 specimens were subjected to annealing in H_2–N_2 atmosphere under the most severe tested conditions (further 5 h at 900 °C). The resulting GIXRD spectrum clearly displayed two intense reflections associated to metallic copper (average cluster size ≈20 nm), without any significant contribution from CuO and/or Cu_2O phases (Fig. 9). Such results were not obtained when *tenorite* was subjected to reducing heat treatments. The different behavior between *tenorite* and *cuprite* could be tentatively explained by considering that the reduction reaction to metal-

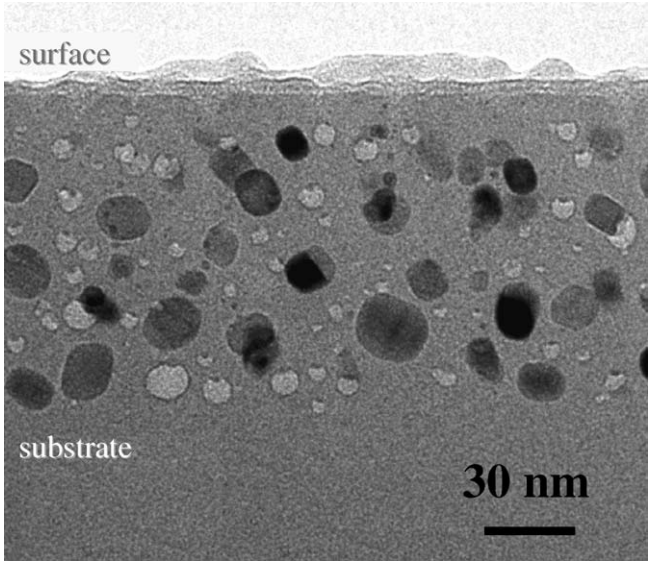

Fig. 6. Representative BF-TEM cross-sectional micrograph for a copper–silica nanocomposites annealed in air at 900 °C for 5 h (adapted from [117]).

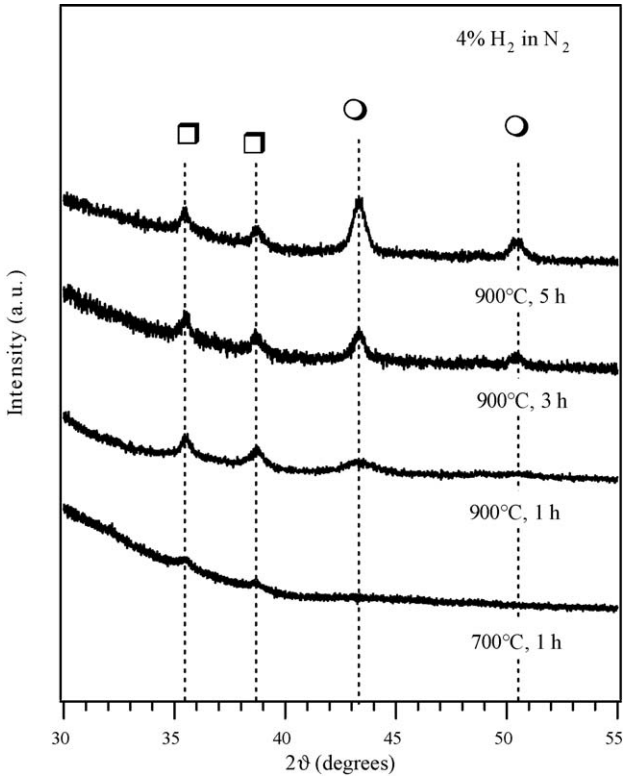

Fig. 7. GIXRD spectra for copper–silica nanocomposites annealed in a 4% H_2–N_2 atmosphere. The markers refer to the CuO (□) and Cu (◯) crystal phases (adapted from [117]).

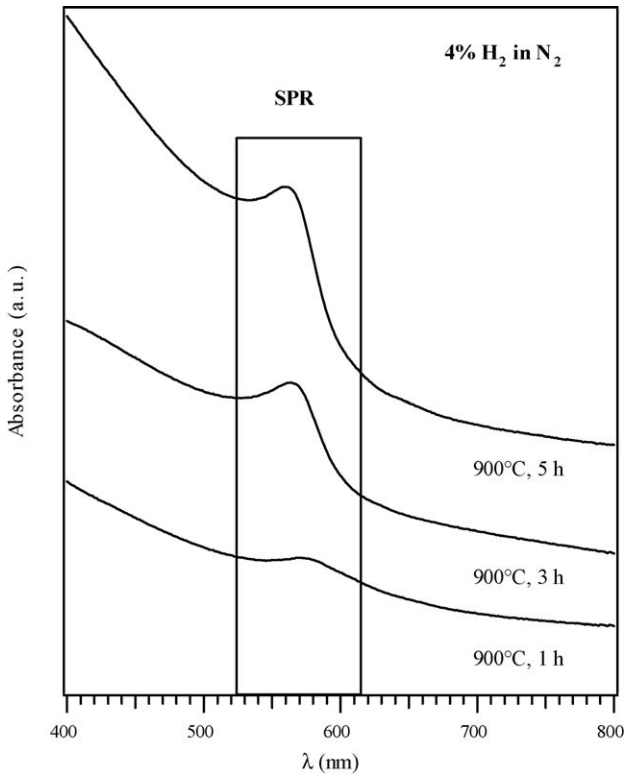

Fig. 8. Optical absorption spectra of copper–silica nanocomposites annealed at 900 °C for different time in a 4% H_2–N_2 atmosphere (adapted from [117]).

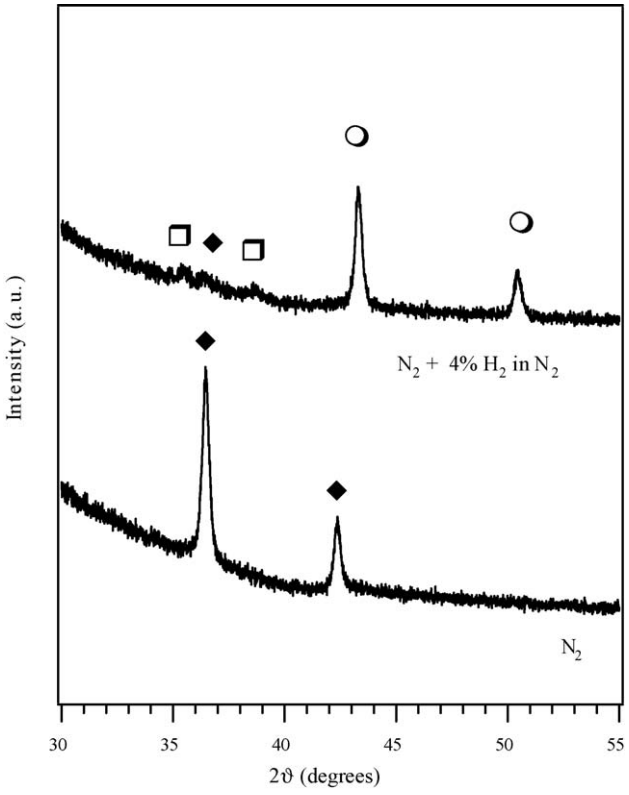

Fig. 9. GIXRD spectra for specimens annealed at 900 °C for 5 h in N_2 and subsequently treated at 900 °C, 5 h in a 4% H_2–N_2 atmosphere. The markers indicate the CuO (□), Cu_2O (♦) and Cu (◯) reflections (adapted from [117]).

lic copper might require different induction times in the two cases.

In order to attain a deeper insight on the NPs structure and composition, the above samples were investigated by TEM analyses. The cluster composition was deduced by HR-TEM and EDS analysis on single particles. In the case of the sample annealed at 900 °C first in N_2 for 5 h and subsequently in H_2–N_2 for 5 h, some of the metallic clusters exhibited a partial *core–shell* structure, in which a Cu *core* was partially surrounded by a CuO *shell*. This structure is shown in the HR-TEM image of Fig. 10, whose Fourier transform indicated the coexistence of (1 1 1) planes of both metallic Cu and CuO in the nanoclusters. To justify the presence of *tenorite*, two explanations can be proposed: (i) a more prolonged treatment for the complete reduction of Cu(II) to Cu(0) is necessary; (ii) the *guest* copper NPs can not be considered as *inert* towards the *host* silica matrix. In fact, atoms lying at the borders can interact with the surrounding oxide medium giving rise to Cu–O bonds, which form a sort of *crown* around the clusters themselves.

Taken together, the results presented in this paragraph have demonstrated the possibility of obtaining copper–silica nanocomposites by a *single-step* SG process. An important feature of the proposed approach is the opportunity to tailor the *guest* phase composition from CuO to Cu_2O and Cu as a function of thermal treatment. In particular, the preparation of homogeneously distributed Cu NPs in a pure silica matrix required the use of severe annealing treatments under reducing atmospheres (4% H_2 in N_2). In these conditions, a complete *host* silica densification was observed, making the matrix undistinguishable from the substrate.

A critical comparison with Ag/SiO_2 systems (Section 3.1) demonstrates important differences and analogies with respect

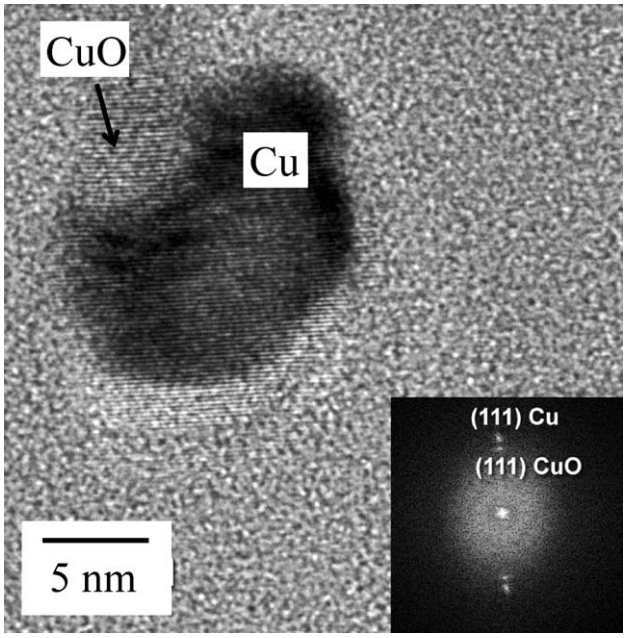

Fig. 10. Representative HR-TEM cross-sectional micrograph and its Fourier transform (inset) for a copper–silica nanocomposites annealed at 900 °C, 5 h in N_2 and subsequently in a H_2–N_2 atmosphere (further 5 h) (adapted from [117]).

to the present case. At variance with Ag/SiO_2 nanocomposites, that were obtained using an amino-functionalized silane capable of originating the silica network and anchoring the silver ions, enabling thus an effective control of Ag NPs size and distribution, Cu/SiO_2 nanosystems were synthesized by exploiting the molecular-level mixing of Cu and SiO_2 precursors in the starting sols. Interestingly, a common feature to both systems was the reactivity of metal NPs towards the *host* matrix promoted by annealing treatments. Concerning Ag/SiO_2 systems, the *host–guest* interaction resulted in the formation of a silver silicate-containing *crown* at the interface between Ag NPs and the surrounding silica. In the case of Cu/SiO_2 nanocomposites, the interaction was more pronounced, leading to the formation of a CuO *shell* around the *guest* Cu particles. As a whole, these characteristics demonstrate the complexity of redox mechanisms controlling the thermal evolution of SG metal NPs-containing composites.

4. *Outside-cluster* systems: Ag/SiO_2 and Au/SiO_2 by RF-sputtering

In the previous section, attention has been focused on the synthesis of Ag/SiO_2 and Cu/SiO_2 *inside-cluster* systems by the SG route, interesting in the field of optics. Nevertheless, applications in catalysis and gas sensing require the metal nanoparticles to be completely, or at least partially, exposed to the ambient in order for the reagents to reach the catalytic centers. While the previously proposed SG strategies are not a viable alternative for the preparation of such composites, RF-sputtering is one of the most versatile techniques for the production of *outside-cluster* systems. In fact, it allows the preparation of supported metal NPs with controllable composition, structure and morphology thanks to the possibility of nucleation to prevail over the subsequent particle growth (Section 2).

The present section focuses on Ag/SiO_2 and Au/SiO_2 *outside-cluster* systems obtained by Ar RF-sputtering of a silver and gold target, respectively, on amorphous silica slides under *soft* synthesis conditions. In general, a controlled modulation of metal content and particle size, shape and distribution was obtained as a function of the applied RF-power, total pressure, substrate temperature and deposition time. Despite the control of such variables could be exerted independently, their *combined* influence strongly affects the system characteristics. In the following, we will try to discuss the role of the different experimental parameters, highlighting the advantages of RF-sputtering in terms of versatility and process control. Particular attention will also be devoted to a comparison of the two systems, with special regard to the characteristics arising from the different chemical reactivity of silver and gold metal NPs.

4.1. Ag/SiO_2 nanosystems

Two of the most important variables influencing sputtering depositions are the RF-power and the total pressure applied to the discharge. While the first affects the dynamics of *collision processes* occurring both in the plasma phase and on the growth surface, the second can be mainly related to the *energy transfer* from the applied electric field to the species present in the discharge, as well as to the target and to the substrate [227]. The mutual interplay of these parameters has to be properly taken into account for a detailed understanding of the plasmochemical processes involved in the NPs nucleation and growth. In particular, variations of p and W influence the value of the so-called self-bias potential, V_{bias}, which is the DC potential developed on the target during plasma ignition [53,228]. This parameter, whose modulus increases with $(W/p)^{1/2}$, is the regulator of the sputtering yield, that increases as V_{bias} becomes more negative [202]. Despite monitoring the self-bias potential is a fundamental mean for an accurate process control, its sole knowledge does not guarantee a complete prediction of the system properties, since the *combined* influence of p and W on both homogeneous and heterogeneous processes has to be considered. To this aim, a precious tool for a deeper insight into the nucleation and growth phenomena resides in the use of in situ characterization techniques, such as LRI, for a *real-time* investigation of the deposition process. This technique monitors the intensity of a monochromatic light beam reflected from the growth surface as a function of t [229] and can probe surface modifications occurring during each growth step [230].

The LRI traces for two representative Ag/SiO_2 sample sets obtained at different total pressures and progressively higher RF-powers are reported in Fig. 11, together with the corresponding V_{bias} value for each sample. A progressive R increase as a function of deposition time from 3.4% (the value for the bare silica substrate [53]) to a final value dependent on the applied RF-power and total pressure was observed, indicating the progressive substitution of the ambience/substrate interface with the more reflecting ambience/silver one. As a general rule, higher final reflectance values were detected on increasing W. Such a result is consistent with the parallel increase of the sputtering yield and, subsequently, of the deposited metal amount, on increasing the modulus of V_{bias}. Furthermore, a careful inspection of Fig. 11 indicates that samples obtained at the same RF-power but different pressures, despite the similar $|V_{bias}|$ values, are characterized by a different final reflectance. This effect is mainly related to the pressure influence on the system properties, affecting both the amount and the morphology of the deposited metal particles [113]. Such considerations are better exemplified by the TEM images reported in Fig. 12 for two samples obtained at the same RF-power, but different p values. While Fig. 12a is characterized by almost spherical and well-separated NPs uniformly distributed on the silica substrate, with a narrow size distribution (average dimensions $\approx$12 nm), a decrease in the total pressure (Fig. 12b) results in a higher density of silver aggregates, characterized by a lower average inter-particle distance. Furthermore, several NPs show marked variations from the spherical shape, and correspondingly, a broader size distribution (10–50 nm). As demonstrated by the image contrast, most particles appear to be composed of several crystallites [60]. These observations, further supported by SAED, GIXRD, AFM and XPS results [113], indicate that a suitable combination of W and p allows a fine modulation of the system composition, structure and morphology, resulting in turn, in a parallel evolution of the optical properties.

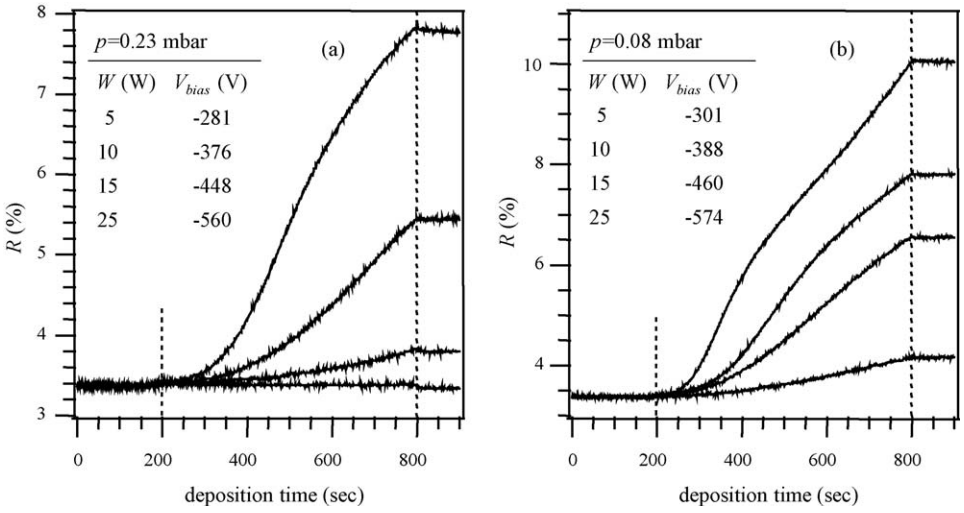

Fig. 11. Reflectance (R, %) vs. t traces obtained by LRI during Ag sputtering on SiO_2 at (a) 0.23 mbar, (b) 0.08 mbar at different RF-powers (from bottom to top: 5, 10, 15 and 25 W; $T = 60\,^{\circ}C$; $t = 10$ min). The vertical lines mark the beginning (plasma on) and the end (plasma off) of the deposition process.

To this regard, the absorption spectra of a representative sample set as a function of the applied RF-power (Fig. 13) are a prototypical example of MDRs [53]. As a general rule, three major effects were detected on going from 5 to 25 W: (i) the appearance and the intensity increase of an absorption band in the visible region, attributable to the SPR of Ag/SiO_2 nanosystems [4,57,118,166]; (ii) a concomitant broadening of the same signal; (iii) a red-shift from $\lambda \approx 450$ to ≈ 550 nm.

The band intensity increase was mainly traced back to the higher sputtering yield on increasing the RF-power, thus resulting in the deposition of a progressively higher metal amount. Moreover, the observed peak broadening was related to a gradually wider NPs size and shape distribution at higher silver percentages [4,7,39]. This phenomenon was likely responsible also for the remarkable peak asymmetry in the samples featuring a higher Ag content [40,166]. Finally, the peak shift towards higher wavelengths was ascribed to the absorption by larger coalescence aggregates [37,39,40,57] and to the increasing interaction between more densely packed Ag NPs [135], resulting in the so-called *island-like* nanosystems [53].

In analogy to Ag/SiO_2 *inside-cluster* nanocomposites (compare Section 3.1), a joint use of XPS and XE-AES analyses was necessary in order to determine the silver oxidation state. In this case, typical values of α_1 and α_2 fell between those reported for Ag(0) and Ag(I) [113,114], suggesting thus a partial surface Ag oxidation. The occurrence of this phenomenon was further confirmed by the analysis of O1s and C1s photoelectron peaks that pointed out to the presence of carbonates/bicarbonates likely arising from interactions of silver NPs with the outer atmosphere [113,114]. Interestingly, the amounts of these species increased on decreasing the Ag NPs dimensions, indicating a direct correspondence between reactivity with outer atmosphere and silver

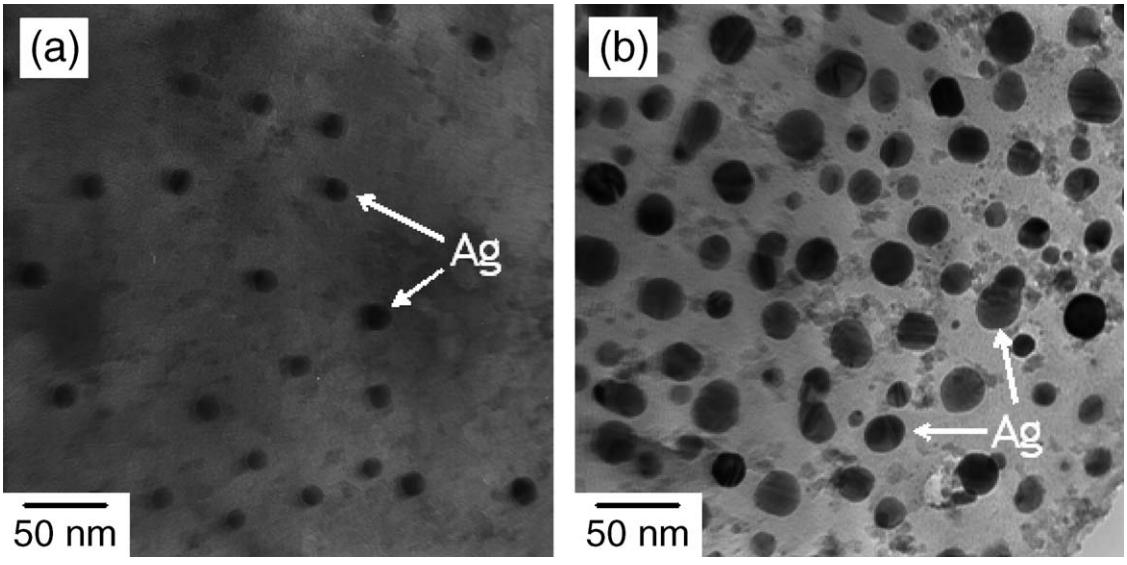

Fig. 12. Plane-view TEM images of two Ag/SiO_2 specimens obtained at 5 W and (a) 0.23 mbar and (b) 0.08 mbar. The corresponding Ag surface atomic percentages were ≈30 and ≈75%, respectively, as determined by XPS analysis (adapted from [113]).

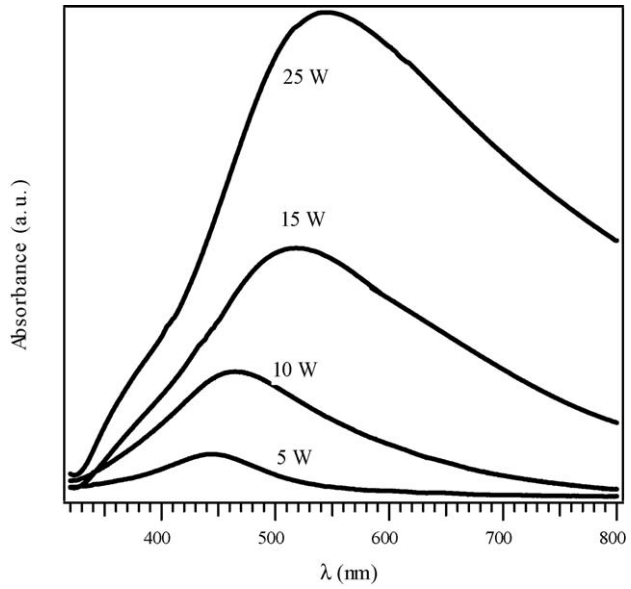

Fig. 13. Optical absorption spectra for an Ag/SiO_2 sample set obtained at $p = 0.23$ mbar and different RF-powers.

cluster size. Nevertheless, despite this partial oxidation, the presence of metallic silver was confirmed by UV–visible and GIXRD results. Such considerations are consistent with the occurrence of metallic Ag NPs surrounded by an oxidized *shell*.

In summary, a critical examination of the results obtained by different analytical in situ and ex situ techniques allowed to elucidate the dynamics of the processes involved in the nucleation and growth of silver on silica, whose evolution could be summarized as follows:

- at the beginning of the sputtering process Ag_n/Ag_n^+ species impinge on the silica surface from the plasma phase, giving rise to small and far apart nucleation sites. During the first stages, i.e., when the deposited silver amount is low enough, very small spherical NPs, with a narrow size distribution, are formed on the SiO_2 surface;
- a progressive increase in the silver content results both in the formation of further nucleation sites and in the growth of pre-formed ones, according to a Volmer–Weber mechanism [113]. This phenomenon produces bigger particles with a broader size distribution and shape variations from spherical-like to prolate. All the above effects and the concomitant lowering of the inter-particle distance result in a steeper increase of the system reflectance and in a stronger absorption band in the visible region, whose intensity, shape and position are directly dependent on the system morphology.

A comparison of these results with the ones pertaining to SG Ag/SiO_2 nanocomposites points out to an appreciable reactivity of Ag NPs with the surrounding medium in both cases (Section 3.1). For the present systems, interaction with the outer atmosphere produces an external carbonate/bicarbonate *shell* around the particles. Conversely, as regards Ag/SiO_2 *inside-cluster* systems obtained by SG, *host–guest* interactions result in a silver silicate *crown* between Ag NPs and the silica matrix. For *outside-cluster* systems, this particle reactivity could be advantageously exploited in functional applications such as heterogeneous catalysis. Nevertheless, it might induce a progressive alteration of the system properties under prolonged use, requiring thus a judicious optimization of the synthesis conditions to stabilize Ag NPs.

4.2. Au/SiO_2 nanosystems

Gold sputtering on silica was performed under different conditions in order to systematically investigate the interplay among the synthesis parameters and the obtained nanosystem properties [53,116]. As already observed in Section 4.1, the appreciable self-bias potential dependence on W [53] could be properly exploited for a careful modulation of the deposited metal amount. Fig. 14a shows a linear increase of the Au surface atomic percentage as a function of the applied RF-power for a representative sample set. A similar behavior, that was also observed at different total pressures [53], is consistent with the increase of the sputtering yield under more drastic plasma conditions. Interestingly, despite the linear interrelation reported in Fig. 14a, other system properties follow a different depen-

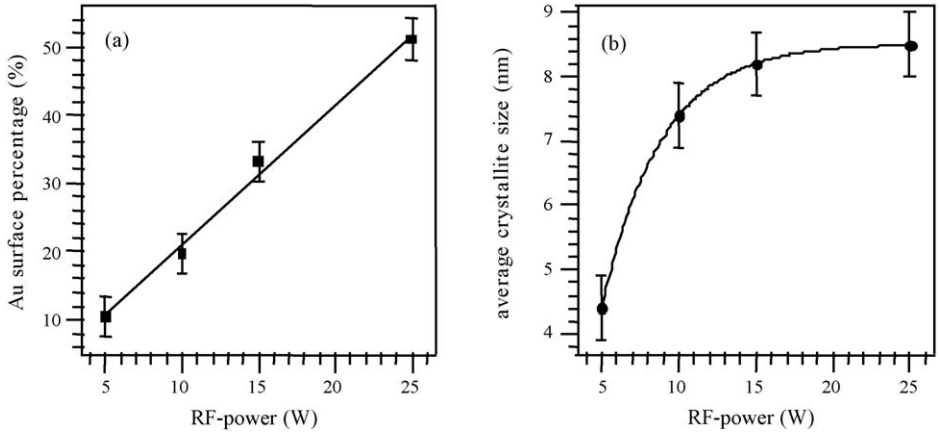

Fig. 14. (a) XPS Au surface percentage and (b) average Au crystallite size vs. RF-power for an Au/SiO_2 sample set ($p = 0.38$ mbar, $T = 60\,^{\circ}C$, $t = 10$ min) (adapted from [53]).

dence on the RF-power. In particular, the average crystallite size, as estimated from GIXRD peak width, presents an exponential increase with W, leading to a sort of saturation regime at the highest W values (Fig. 14b). Such a behavior can be traced back to the predominance of nucleation over the subsequent NPs growth, despite the progressive increase in the sputtering yield with power. In fact, an important feature of the RF-sputtering technique is the competition between deposition and ablation processes characterizing glow discharges [53,74,203], the latter becoming progressively more important at higher W values. This aspect represents a key factor for the synthesis of supported NPs with tailored structure/morphology, which in turn, strongly affect their optical properties.

A further tailoring of the system features could be achieved by controlling the sputtering time and deposition temperature [116]. In particular, while variations of t allow to elucidate the temporal dynamics of nucleation/coalescence processes as a function of the metal content, T has a strong influence on gold NPs surface distribution and crystallinity, as well as on their size and shape.

The structural evolution for two representative sample sets as a function of t and T is reported in Fig. 15a and b, respectively. As a general rule, diffraction patterns are characterized by the signals of fcc metallic gold, with no appreciable preferential orientation. In particular, as concerns Fig. 15a, variations of the peak intensity are related to the increase of the deposited metal amount with t, all the other parameters being constant. In this context, the absence of clearly detectable signals for the sample obtained at 5 min can be mainly traced back to the low gold content (≈5% Au surface atomic percentage, as obtained by XPS analysis) [116]. Higher sputtering times resulted in the linear increase of the Au surface percentage (up to ≈25% for sample obtained at 30 min) [116]. Interestingly, in the present case, the average crystallite size displayed a linear (and not exponential, like in Fig. 14b) increase on increasing t from 5 to 30 min [231]. This phenomenon can be related to the preferential interaction of impinging Au-containing species with pre-formed gold nucleation sites rather than with silica, in agreement with a Volmer–Weber growth mechanism (see below) [167,179,232]. The different dependence of the crystallite size on deposition time and RF-power is consistent with the different role exerted by such parameters on the material properties, since the applied RF-power also influences the competition between deposition and ablation phenomena.

In the case of Fig. 15b, all specimens are characterized by the same deposited metal amount. As a consequence, the progressive intensity increase and peak narrowing of gold reflections with deposition temperature can be ascribed to thermal diffusion of Au species and subsequent coalescence into bigger NPs [94,233]. Such events are likely enhanced by particle bombardment on the growth surface during the depositions, that is expected to favor the re-distribution of gold species. In fact, a linear increase of the crystallite size on increasing T from 60 to 210 °C is demonstrated and accompanied by a variation of the Au surface atomic percentage from ≈20 to ≈40% [116], indicating an augmented dispersion of Au NPs on SiO_2. For these specimens, AFM investigation (Fig. 16) reveals a globular surface morphology, typical for a 3D Volmer–Weber growth mechanism [167,179,232].

Interestingly, a common feature to all the obtained Au/SiO_2 *outside-cluster* nanosystems is the absence of Au NPs reactivity with their surroundings. In fact, XPS analyses never demonstrate the presence of species different from Au(0), irrespective of the processing conditions. Such a feature points out to a relatively higher stability of the obtained gold NPs with respect to the Ag ones (Section 4.1) and to negligible interactions with their surroundings.

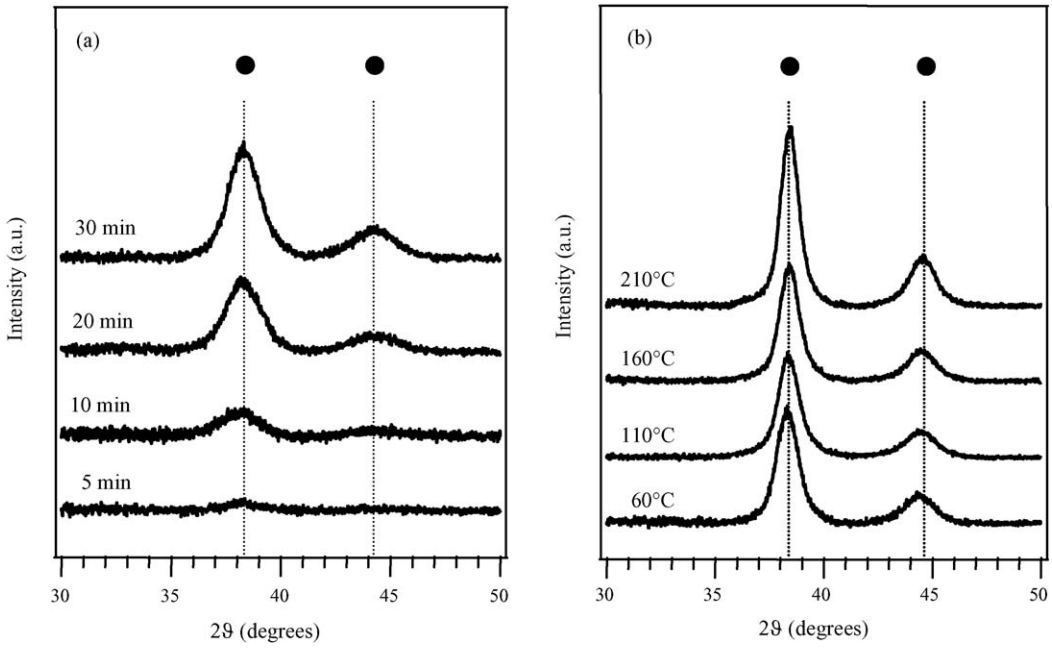

Fig. 15. GIXRD patterns of Au/SiO_2 nanosystems as a function of (a) sputtering time (W = 5 W, p = 0.38 mbar, T = 60 °C, V_{bias} = −250 V) and (b) substrate temperature (W = 10 W, p = 0.38 mbar, t = 20 min, V_{bias} = −355 V). The vertical lines indicate the peak positions for bulk gold (adapted from [116]).

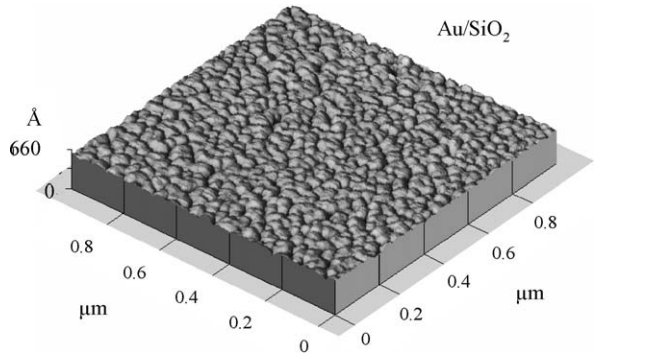

Fig. 16. Representative AFM image (1 μm × 1 μm) for an as-prepared Au/SiO_2 specimen ($W = 10$ W, $p = 0.38$ mbar, $T = 60\,^{\circ}C$; $t = 20$ min). The average grain size is ≈50 nm (adapted from [116]).

Selected TEM images of two representative samples are reported in Fig. 17. In Fig. 17a, the presence of gold nanoclusters with an average size of 3–4 nm can be observed. Most of the NPs appear single-domain, almost spherical in shape and quite separated from each other. Conversely, the sample in Fig. 17b displays a uniform dispersion of elongated and bigger Au aggregates. Interestingly, the image contrast suggests that such NPs are multi-domain [2] (average crystallite size ≈5 nm), as indicated by the darker spots clearly visible in several agglomerates.

Such specimens can be considered the prototype of two different nanosystems, the so-called *cluster-* or *island-like* systems, respectively [53], characterized by diversified optical responses. In fact, while the sample of Fig. 17a presents the typical SPR peak expected in the case of well dispersed gold NPs in/on a dielectric medium, the morphology of Fig. 17b results in a broadened and asymmetric absorption band extending towards the IR region. In analogy to the case discussed in Section 4.1 (see also Fig. 13), this is another characteristic example of MDRs, revealing a direct influence of the system morphology on the resulting optical response.

In summary, a careful choice of the operational parameters (RF-power, total pressure, substrate temperature and deposition time), together with a thorough understanding of their influence on the deposition process, enables to control both the morphology and the optical properties of the obtained Au/SiO_2 nanocomposites.

5. Between *inside-* and *outside-clusters*: Au/TiO_2 by an hybrid RF-sputtering/sol–gel approach

We focus now the attention on Au/TiO_2 nanosystems synthesized by an original hybrid RF-sputtering/SG route [111], as described in Section 2. In particular, titania xerogels (*host*) were deposited on silica slides by dip-coating from ethanolic solutions containing titanium(IV) isopropoxyde and acetylacetone. The obtained specimens, free from any detectable crystalline phase as proved by GIXRD analyses, were subsequently used in RF-sputtering depositions of gold (*guest*) from Ar plasmas without further treatments. Experiments were carried out under optimized conditions, at temperatures as low as 60 °C, in order to avoid thermally induced modifications of the *host* xerogel morphology and structure.

The overall sputtered gold amounts in the obtained specimens was tailored by varying the V_{bias} values during the sputtering processes. The as-prepared specimens displayed a color dependence on the synthesis conditions, changing from green to pink on decreasing the Au content. In order to investigate heat-induced structural, compositional and morphological evolutions, all the samples were annealed ex situ in air for 1 h at temperatures ranging from 200 to 600 °C. In principle, thermal treatment could induce either a coalescence of the *guest* Au particles in the near-surface region or their migration in the inner layers of the *host* TiO_2 matrix. It is worth noticing that the plasma treatment itself did not induce the crystallization of the as-prepared titania xerogels, which transformed into nanostructured *anatase* (mean crystallite size ≈15 nm) only after thermal treatments at

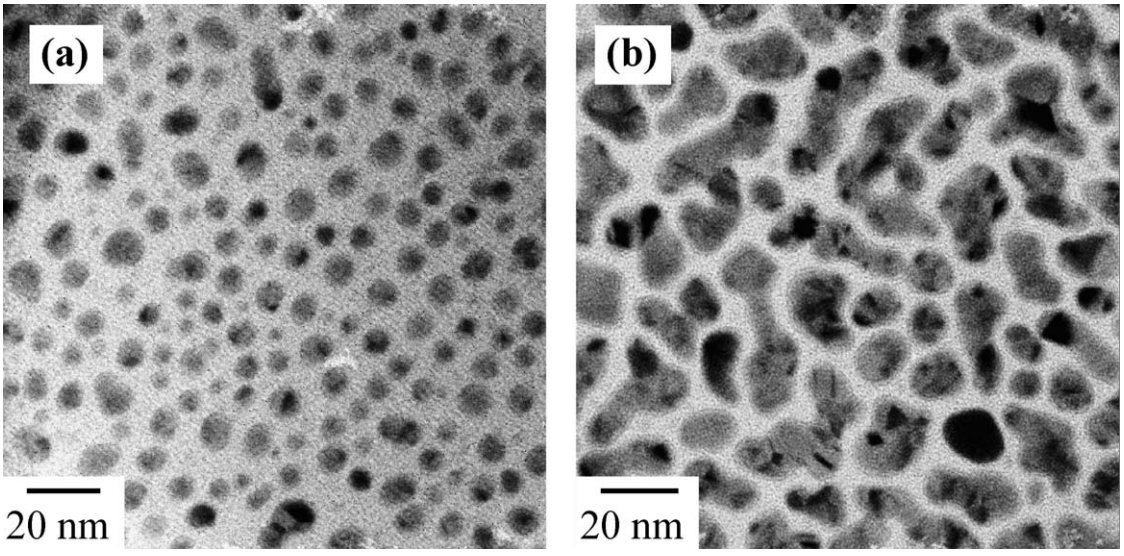

Fig. 17. BF-TEM images for Au/SiO_2 nanosystems obtained at: (a) $W = 5$ W, $p = 0.38$ mbar, $T = 60\,^{\circ}C$, $t = 30$ min; (b) $W = 5$ W, $p = 0.08$ mbar, $T = 60\,^{\circ}C$, $t = 10$ min (adapted from [53]).

$T \geq 400\,^{\circ}C$, as typically observed for TiO_2 films synthesized by the SG route [152,153,173,234].

Irrespective of the processing conditions, a progressive decrease of the Au surface percentage with the annealing temperature was observed (Fig. 18a). Moreover, the dependence of Au content on T became progressively weaker on lowering the overall gold amount in the as-prepared specimens (i.e., on lowering the $|V_{bias}|$ value). This behavior was explained by taking into account that the coalescence/agglomeration of gold NPs, favored by an increase of thermal energy [8,162,174,203], might be responsible for a diminished surface coverage at higher treatment temperatures, resulting in an apparent lowering of Au percentage. Such behavior was expected to be more effective for nanosystems characterized by a higher gold content (Fig. 18a). An additional contributing effect might result from gold penetration in the sub-surface titania layers. Indeed, XPS analyses confirmed the occurrence of this phenomenon already in the as-prepared specimens, that might thus be regarded as mid-way between *outside-* and *inside-cluster* systems (Fig. 1). For the composites containing the lowest gold amount, the weaker variations of Au surface percentage with the heating temperature were related to more limited coalescence/agglomeration processes resulting, in turn, from the lower density of gold NPs in the as-prepared specimens. In this case, appreciable Au percentage variations began to occur at 400 °C, in concomitance with the formation of crystalline TiO_2 [153,235].

Thermally induced gold agglomeration, resulting in the decrease of surface gold content, was confirmed by both GIXRD and TEM analyses. As a general trend, all specimens presented reflections attributed to fcc metal gold, whose intensity underwent a progressive increase under more severe annealing conditions. The mean Au nanocrystal dimensions (Fig. 18b) increased linearly with annealing temperature, indicating that heat treatments favored a progressive coalescence of gold NPs. Interestingly, despite the fact that the average gold crystallite size was ≈4 nm in all the as-prepared specimens, the curve slope increased with the overall Au amount, indicating its appreciable influence on particle agglomeration, as suggested above.

A deeper insight into the Au/TiO_2 nanostructure as a function of thermal treatment was obtained by TEM analyses. Fig. 19a and b report representative micrographs of an as-prepared specimen. On the surface of the titania film, Au particles having a bimodal size distribution can be clearly discerned. The smallest clusters had a mean diameter lower than 2 nm and a higher population density, whereas largest particles between 5 and 8 nm were also present (Fig. 19a). The higher number of smaller particles was attributed to the peculiar composition of the titania *host* matrix, i.e., to the presence of polar groups (mainly −OH), acting as grafting sites for the sputtered gold particles (Section 2) [111]. This feature, together with the *soft* deposition conditions ($T = 60\,^{\circ}C$), is likely to result in the formation of many nucleation sites per unit area, that limit the subsequent particle agglomeration and growth during the synthesis. An inspection of the HR-TEM image in Fig. 19b allowed to discern the (1 1 1) planes of fcc metal gold and the amorphous structure of the titania matrix, in agreement with GIXRD results.

As a matter of fact, a significant structural evolution was observed upon thermal treatment in air. Fig. 19c and d display two selected TEM images for the sample of Fig. 19a and b after annealing at 600 °C. As can be noticed, heat treatment produced the crystallization of the titania *host* matrix (fringes due to (1 0 1) *anatase* planes are evident) and the growth of larger gold particles at expenses of smaller ones, whose numerical density underwent a remarkable decrease. Moreover, most Au NPs appeared to be composed by the aggregation of different nanocrystallites, as proved by the image contrast in Fig. 19d.

In analogy to the results reported in Section 4.2, XPS investigation demonstrated that Au NPs only contained metallic gold species, whatever the adopted conditions.

The Au/TiO_2 system evolution as a function of the annealing temperature was further investigated by optical spectroscopy, as exemplified in Fig. 20. As can be observed, the absorption spectrum of the as-prepared Au/TiO_2 system showed a broadened

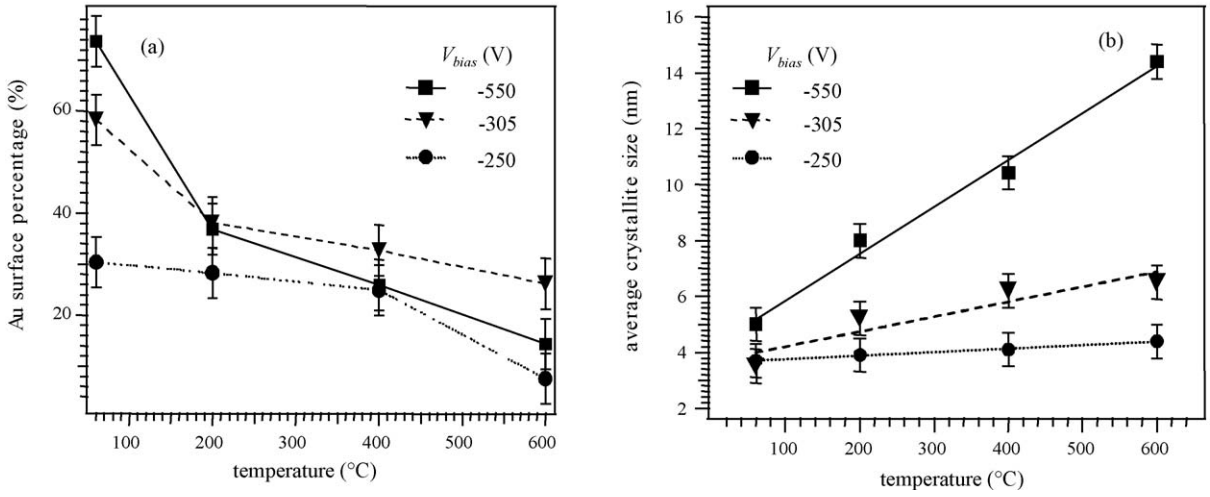

Fig. 18. (a) Evolution of gold percentage and (b) mean Au crystallite size for Au/TiO_2 nanocomposites as a function of the annealing temperature. Gold content in the different samples was tailored by changing the V_{bias} value in the sputtering experiments (adapted from [111]).

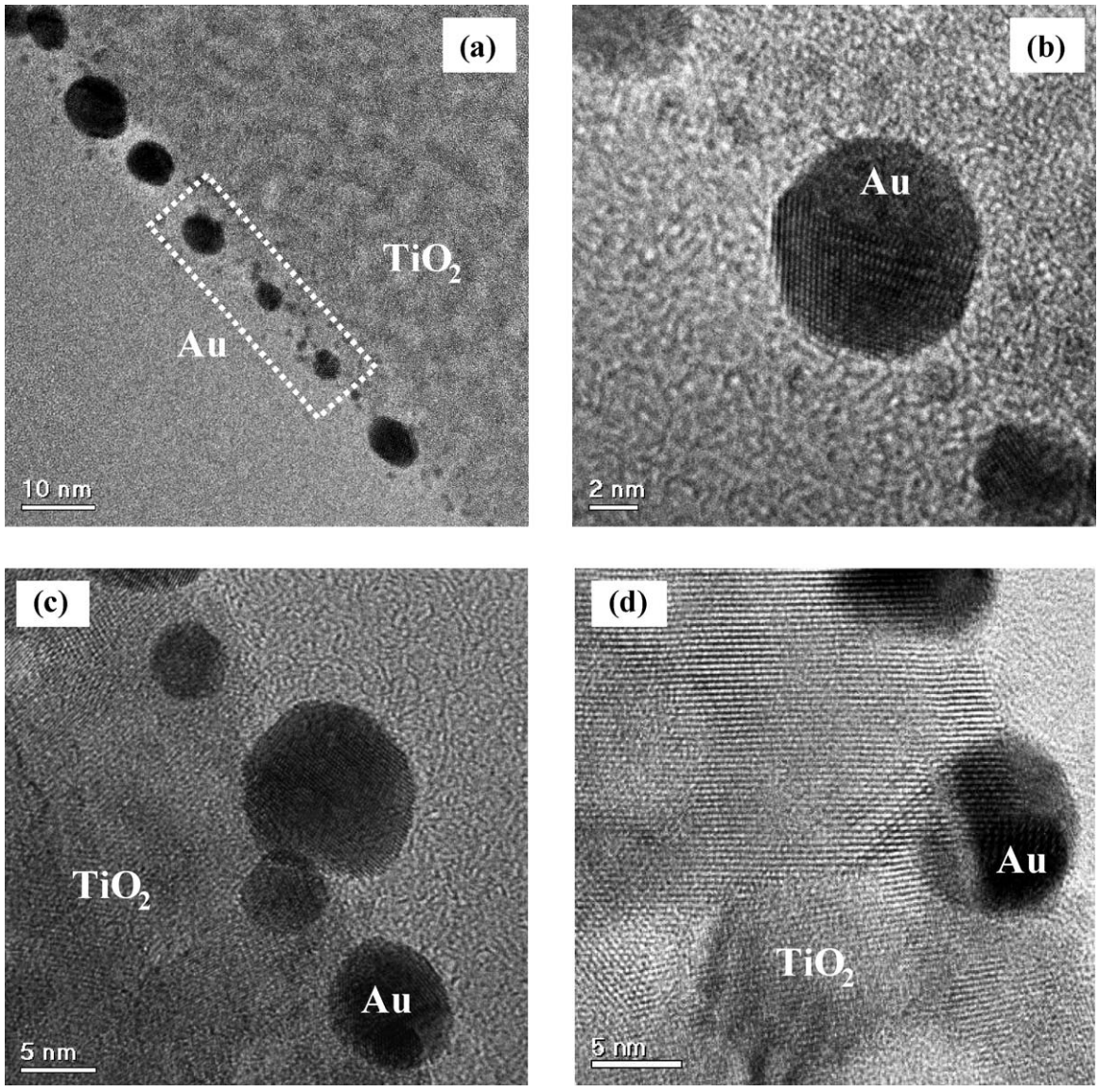

Fig. 19. BF-TEM images for an Au/TiO_2 sample obtained at $V_{bias} = -305$ V ($W = 5$ W, $p = 0.08$ mbar, $T = 60\,^{\circ}C$, $t = 10$ min): (a and b) as-prepared and (c and d) after annealing in air at 600 °C for 1 h.

band centered at $\lambda \approx 640$ nm extending towards the IR region, characteristic for an Au/TiO_2 nanosystem with a very large particle size distribution [109]. Similar spectra have already been discussed for *island-like* nanosystems (Section 4). Upon annealing (200 °C), the development of a SPR peak centered at $\lambda \approx 590$ nm, typical for gold nanoclusters dispersed in/on a titania matrix, was observed [77,152,153]. At higher treatment temperatures, the plasmon band underwent an intensity increase and a progressive shift to higher wavelengths, up to $\lambda \approx 630$ nm. Similar red-shifts have been mainly attributed to the change in the relative permittivity of the *host* TiO_2 matrix upon crystallization [8,50,77,153,162,174,203].

The above results demonstrated that the chemico-physical properties of Au/TiO_2 nanosystems obtained by the hybrid RF-sputtering/SG approach are strongly affected by: (i) the overall gold amount in the starting specimens, influencing the system thermal evolution; (ii) the *active* role of the SG titania xerogel in tailoring the Au NPs distribution. For samples containing the lowest Au amount, small gold NPs can be considered homogeneously dispersed on the xerogel surface and partially trapped in the matrix pores, thus preventing an appreciable coalescence of Au agglomerates. At progressively higher gold content, the overall contact area between different Au NPs is likely to increase, so that thermally induced coalescence/agglomeration processes are more favored. Such features can explain the different dependence of Au surface percentage and nanocrystal size on temperature (Fig. 18).

6. From metal nanoclusters to nanotubes: RF-sputtering of gold into porous membranes

In the previous paragraphs, attention has been focused on nanocomposites containing both supported and embedded metal NPs. To this aim, tailoring of the particle size and shape [123],

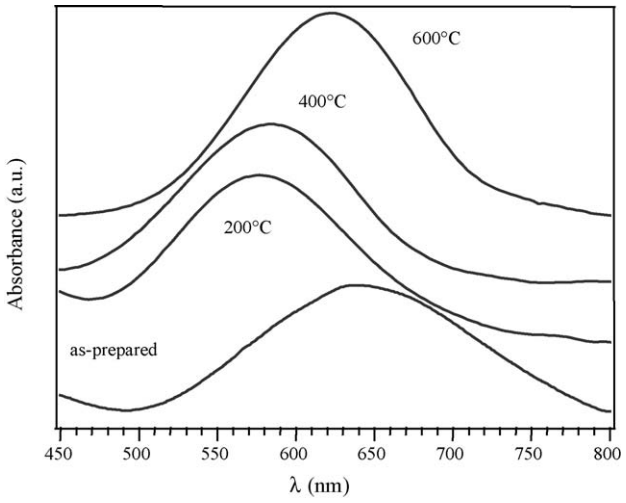

Fig. 20. Evolution of optical absorption spectra with annealing temperature for Au/TiO_2 specimens obtained at $V_{bias} = -305$ V ($W = 5$ W, $p = 0.08$ mbar, $t = 10$ min, $T = 60$ °C) (adapted from [111]).

as well as of their surface and in-depth distribution, has been shown to be particularly important in order to control the system properties and achieve specific functional performances. In this context, several research efforts have been addressed to obtain metal 1D nanosystems, especially based on gold [123,236]. Among the various synthetic approaches, template routes entailing the synthesis of 1D metal nanostructures in suitable membranes have received a great attention [58,129,237,238]. Following this philosophy, the desired metal-based architecture is obtained by controlling the assembly of metal NPs within the pores of the membrane, whose channel structure and morphology direct the 1D growth. Finally, the template can be selectively removed by means of post-synthesis chemical processes [121]. Depending on the membrane and the specifically adopted method, either nanorods or hollow nanotubes with tailored aspect ratio (length/diameter) and functional properties can be obtained [239].

Basing on our previous works concerning the RF-sputtering of gold on conventional substrates [53,116], in the present paragraph we demonstrate the possibility of transferring such results to the vapor-phase synthesis of 1D gold NTs by controlling the in-depth distribution and organization of gold NPs in the pores of AAO *hosts*. To this aim, the tailored dispersion of metal particles in the AAO membrane (Fig. 21) used as a sacrificial template and their controlled organization allows the preparation of both Au/AAO composites and free-standing gold 1D nanostructures, the latter being obtained by ex situ *host* removal in acidic or alkaline aqueous solutions.

An important method advantage is the possibility to achieve the conformal coverage of a complex surface topography under low-temperature conditions. In particular, the infiltration power and the competition between deposition and ablation processes characterizing plasma-assisted techniques [53] enable to tailor the penetration of gold NPs into the AAO membranes and their controlled assembly into 1D nanostructures, whose morphology depends on the synthesis conditions and the membrane pore size.

The method potentials are exemplified by the SEM micrographs reported in Fig. 22. In fact, despite the presence of non-regular channels, the in-depth gold penetration into the AAO membrane was demonstrated by the cross-section image of Fig. 22a, where the chemical contrast suggested the presence of Au in a region ≈1 μm thick. Interestingly, a higher magnification micrograph (Fig. 22b) revealed that pore filling occurred as a result of the decoration of the AAO pore walls by gold NPs of a few tenths of nanometers (mean gold crystallite size ≈25 nm). The coalescence of such aggregates, whose formation was studied in detail in our previous works [53,111,116], in the outermost AAO membrane regions resulted in 1D structures with a shape complementary to that of the matrix pores and an aspect ratio close to five.

In order to attain a deeper insight into gold nanotube morphology, our interest was subsequently devoted to obtain a controlled template removal, enabling to preserve the original morphology of Au 1D nanoaggregates. Membrane etching in aqueous sodium hydroxide solutions [128,236,240,241] allowed an efficient AAO dissolution and demonstrated a uniform distribution of self-supporting and aligned Au 1D nanostructures (Fig. 23). Interestingly, most of them present a conical-like shape complementary to that of the membrane pores. Differently from most 1D Au nanosystems previously obtained in AAO [58,122,240,242], most of the present structures appear open at the top, thus proving the formation of NTs instead of nanowires/rods. This feature, demonstrating the conformal coverage achievable by the proposed synthetic pathway, could be of relevant importance in several applicative fields [236].

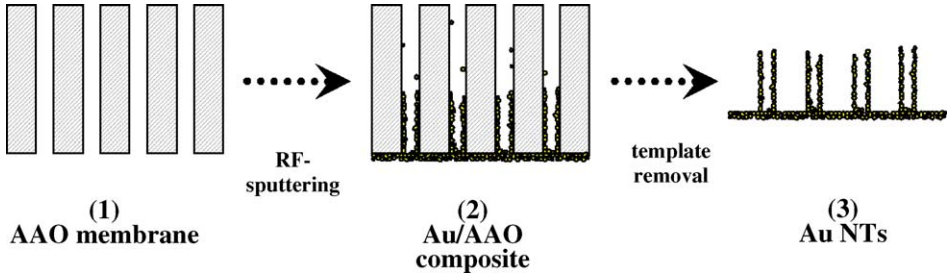

Fig. 21. Sketch of the procedure adopted for the synthesis of gold nanotubes. An AAO membrane (nominal pore diameter = 200 nm) (1) is subjected to RF-sputtering of gold from Ar plasmas ($W = 40$ W; $p = 0.02$ mbar; $t = 60$ min) at temperatures as low as 60 °C, resulting in the formation of an Au/AAO composite (2). Ex situ etching of the template in acidic or alkaline solutions enables to release self-supporting Au tubules (3) (adapted from [236]).

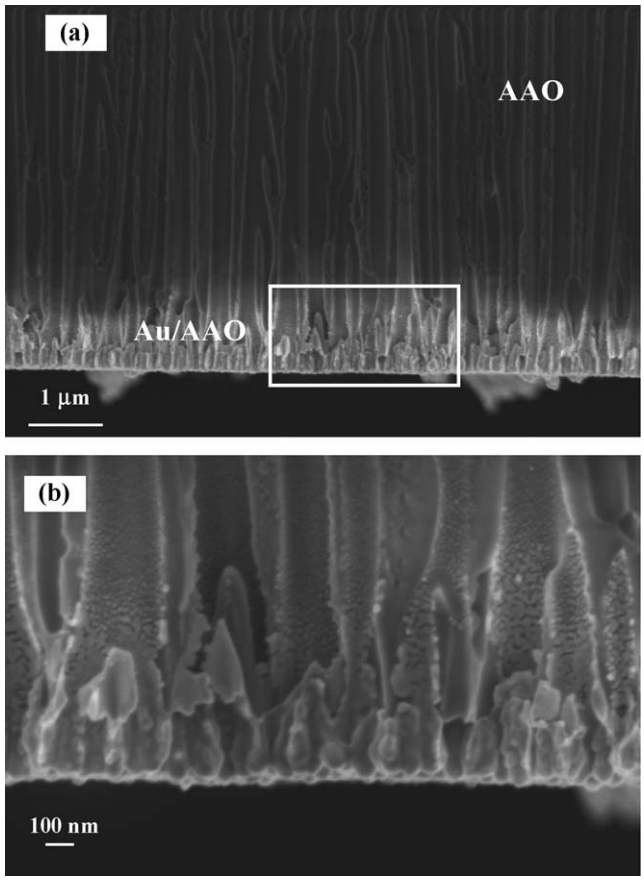

Fig. 22. (a) Cross-section SEM micrograph of an as-prepared Au/AAO specimen displaying both the pore filling by Au NPs (brighter region) and the AAO porous structure (darker area). (b) Enlarged view of the box demonstrated in (a) (adapted from [236]).

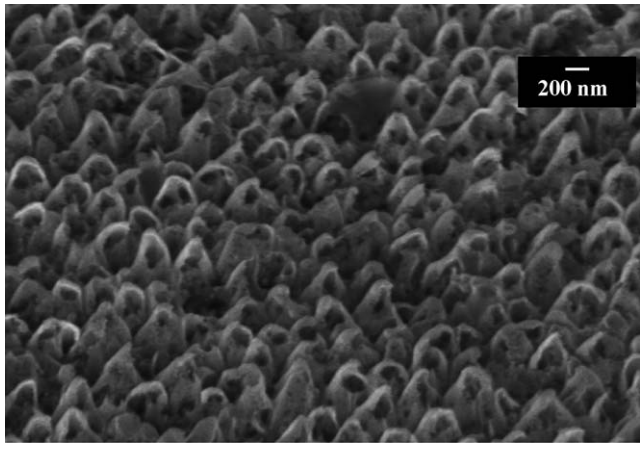

Fig. 23. Representative SEM image of self-supporting gold NTs obtained after AAO membrane etching in an aqueous NaOH solution (adapted from [236]).

7. Concluding remarks and future outlook

This review was focused on functional nanocomposites based on 11th group metal NPs (Cu, Ag and Au, *guest*) in/on oxide matrices (SiO_2, TiO_2, Al_2O_3, *host*). Although the tailoring of elemental composition and size for NPs has been a key issue over the last decade, their controlled assembly into hierarchically organized structures is nowadays an important tool to tune the chemistry and physics of these systems. As a consequence, the research activities dedicated to the development of *bottom-up* strategies for tailoring the nano-units nucleation and their subsequent spatial organization have enormously enriched. In this context, our main aim was to present our recent results on Cu, Ag and Au NPs-containing systems obtained by solution- and vapor-phase routes, namely SG, RF-sputtering and their innovative combinations. Both techniques represent versatile synthetic approaches to metal NPs-based materials, since they typically operate under non-equilibrium conditions, where nucleation is predominant over the subsequent particle growth. While the SG route is particularly suitable in obtaining metal NPs *inside* an oxidic matrix by a *single-step* process, RF-sputtering is an amenable approach for the deposition of metal clusters on the outer surface of a given substrate (*outside-cluster* systems). Moreover, if an as-prepared SG material is used as an active support for RF-sputtering depositions, the resulting hybrid preparation strategy presents inherent advantages for the production of *host–guest* nanocomposites with peculiar features under *soft* and controlled conditions. In this context, the RF-sputtering technique can also be used for the dispersion of metal NPs into suitable oxidic membranes provided with 1D channels, where the particle assembly can lead to more complex organized structures (composite-containing or free-standing metal NTs). A similar variety of systems, whose features can be controlled at a nanometric level by a proper choice of experimental parameters and ex situ annealing conditions (temperature, time, atmosphere), is of great interest for the production of advanced functional devices with prescribed performances.

With regard to the Cu-, Ag- and Au-based nanocomposites discussed in the present review, one of the main points emerging from the presented results is related to the different reactivity of metal NPs with their surroundings, i.e., with the *host* matrix (*inside-clusters*) or the external atmosphere (*outside-clusters*). In the case of all gold NPs-containing systems, only metallic Au species were detected, pointing out to negligible interactions of gold nanoclusters with the surrounding medium. In a different way, investigation on SG Ag/SiO_2 nanosystems revealed the occurrence of some interactions between silver NPs and the silica matrix, related to the presence of oxidized silver species and to the formation of a silicate *shell* surrounding the nanoclusters. The reactivity of Ag NPs was also confirmed for Ag/SiO_2 *outside-cluster* systems obtained by RF-sputtering, that showed the presence of chemical species different from the sole metallic silver, mainly attributed to carbonates or bicarbonates arising from atmospheric exposure. As a general rule, lower silver particle sizes corresponded to more enhanced reactivity with the surroundings. Finally, the production of SG copper–silica nanocomposites almost free from oxide phases (Cu_2O, CuO) required ex situ thermal treatments in reducing atmospheres under adequate conditions. Even in this case, the formed copper NPs cannot be considered as *inert* towards the silica matrix, as demonstrated from the presence of oxide *crowns* surrounding the particles themselves.

In conclusion, the extraordinary variety of structure and properties for M'/M_xO_y nanocomposites paves the way to further

research developments. An attractive possibility is the synthesis of supported bimetallic NPs, such as Au–Ag, paying special attention to mechanisms leading to the alloy formation as a function of the synthesis conditions and to the dependence of the optical properties on the mutual content of the two metals. In this context, further interesting developments might concern the controlled assembly of Au–Ag NPs in 1D nanostructures by the template approach proposed in this review. Specifically, the control of the relative Au/Ag amount can provide an effective tool for a chemical modulation of the system properties. To this aim, such bimetallic systems result interesting for the investigation of catalytic performances and their interrelations with the system properties, which in turn, strongly depend on the processing parameters. Moreover, the derivatization of Au NTs with molecular species such as SMMs might open interesting perspectives for the development of advanced devices for information storage and transmission. In this context, the evaluation of the Au NTs magnetic properties, which might significantly depend on the peculiar NTs size and shape, also anticipates innovative functional applications. Undoubtedly, the above-proposed examples represent only a part of the exciting and fascinating possibilities concerning future trends on the nanoengineering of nanomachines, clusters and functional structures, whose thorough exploitation might revolutionize many current industrial processes and well-established technologies.

Acknowledgments

National Research Council (CNR), University of Padova and INSTM are acknowledged for financial support. We are also indebted to research programs FISR-MIUR "Molecular nanotechnologies for information storage and transmission", FISR-MIUR "Inorganic and hybrid nanosystems for the development and innovation of fuel cells" and FIRB-MIUR-RBNE019H9K "Molecular manipulation for nanometric machines". Thanks are also due to Prof. S. Gialanella (Department of Materials Engineering and Industrial Technologies, University of Trento, Trento, Italy), Dr. G. Mattei (INFM and Department of Physics, University of Padova, Padova, Italy) and Prof. S. Polizzi (Department of Physical Chemistry, Ca' Foscari Venice University, Venice, Italy) for TEM analyses, and to Dr. C. Sada (INFM and Department of Physics, University of Padova, Padova, Italy) for thickness measurements. Finally, we acknowledge Dr. M. Del Marro, Dr. E. Garofalo and Mr. G. Pallocca (Assing Research Center, Rome, Italy) for SEM measurements.

References

[1] K.E. Drexler, Nanosystems: Molecular Machinery, Manufacturing, and Computation, J. Wiley & Sons, New York, 1992.
[2] M. Hirasawa, H. Shirakawa, H. Hamamura, Y. Egashira, H. Komiyama, J. Appl. Phys. 82 (1997) 1404.
[3] G. Schmid, J. Chem. Soc., Dalton Trans. 7 (1998) 1077.
[4] T. Wenzel, J. Bosbach, F. Stietz, F. Träger, Surf. Sci. 432 (1999) 257.
[5] C. Charton, M. Fahland, Surf. Coat. Technol. 174–175 (2003) 181.
[6] J.J. Mock, M. Barbic, D.R. Smith, D.A. Schultz, S. Schultz, J. Chem. Phys. 116 (2002) 6755.
[7] W. Cai, H. Hofmeister, M. Dubiel, Eur. Phys. J. D 13 (2001) 245.
[8] W. Cai, H. Hofmeister, T. Rainer, W. Chen, J. Nanopart. Res. 3 (2001) 443.
[9] R.N. Barnett, C.L. Cleveland, H. Häkkinen, W.D. Luedtke, C. Yannouleas, U. Landman, Eur. Phys. J. D 9 (1999) 95.
[10] R. Jin, Y.-W. Cao, C.A. Mirkin, K.L. Kelly, G.C. Schatz, J.G. Zheng, Science 294 (2001) 1901.
[11] Z. Pászti, G. Petö, Z.E. Horváth, O. Geszti, A. Karacs, L. Guczi, Nucl. Instrum. Methods Phys. Res., Sect. B 178 (2001) 131.
[12] J. Zhu, S. Liu, O. Palchik, Y. Koltypin, A. Gedanken, Langmuir 16 (2000) 6396.
[13] A. Wolf, F. Schüth, Appl. Catal. A 226 (2002) 1.
[14] P. Innocenzi, G. Brusatin, A. Martucci, K. Urabe, Thin Solid Films 279 (1996) 23.
[15] C.N.R. Rao, G.U. Kulkarni, P.J. Thomas, P.P. Edwards, Chem. Soc. Rev. 29 (2000) 27.
[16] C. Burda, X. Chen, R. Narayanan, M.A. El-Sayed, Chem. Rev. 105 (2005) 1025.
[17] M. Xiao, Phys. Lett. A 288 (2001) 37.
[18] K.K. Cashwell, C.M. Bender, C.J. Murphy, Nano Lett. 3 (2003) 667.
[19] M.C. Daniel, D. Astruc, Chem. Rev. 104 (2004) 293.
[20] M. Haruta, Catal. Today 36 (1997) 153.
[21] M. Mavrikakis, P. Stoltze, J.K. Nørskov, Catal. Lett. 64 (2000) 101.
[22] A. Henglein, Chem. Rev. 89 (1989) 1961.
[23] G. Schmid, Clusters and Colloids: From Theory to Applications, VCH, New York, 1994.
[24] M.P. Mallin, C.J. Murphy, Nano Lett. 2 (2002) 1235.
[25] Y. Kim, R.C. Johnson, J. Li, J.T. Hupp, G.C. Schatz, Chem. Phys. Lett. 352 (2002) 421.
[26] K. Kim, K.L. Kim, S.J. Lee, Chem. Phys. Lett. 403 (2005) 77.
[27] S.L. Logunov, T.S. Ahmadi, M.A. El-Sayed, J.T. Khoury, R.L. Whetten, J. Phys. Chem. B 101 (1997) 3713.
[28] Y. Guari, C. Thieuleux, A. Mehdi, C. Reye, R.J.P. Corriu, S. Gomez-Gallardo, K. Philippot, B. Chaudret, Chem. Mater. 15 (2003) 2017.
[29] S. Link, Z.L. Wang, M.A. El-Sayed, J. Phys. Chem. B 103 (1999) 3529.
[30] R. Persuad, T.E. Madey, in: D.A. King, D.P. Woodruff (Eds.), The Chemical Physics of Solid Surfaces and Heterogeneous Catalysis, vol. 8, Elsevier, Amsterdam, 1997.
[31] A. Vittadini, A. Selloni, J. Chem. Phys. 117 (2002) 353.
[32] D. Davidović, M. Tinkham, Phys. Rev. Lett. 83 (1999) 1644.
[33] M. Valden, X. Lai, D.W. Goodman, Science 281 (1998) 1647.
[34] G. Petö, G.L. Molnár, Z. Pászti, O. Geszti, A. Beck, L. Guczi, Mater. Sci. Eng. C 19 (2002) 95.
[35] W. Cai, L. Zhang, H. Zhong, G. He, J. Mater. Res. 13 (1998) 2888.
[36] L. Gang, B.G. Anderson, J. van Grondelle, R.A. van Santen, Appl. Catal. B 40 (2003) 101.
[37] K.-P. Charlè, L. König, S. Nepijko, I. Rabin, W. Schulze, Cryst. Res. Technol. 33 (1998) 1085.
[38] E. Traversa, M.L. Di Vona, P. Nunziante, S. Licoccia, T. Sasaki, N. Koshizaki, J. Sol–Gel Sci. Technol. 19 (2000) 733.
[39] H. Hövel, S. Fritz, A. Hilger, U. Kreibig, M. Vollmer, Phys. Rev. B 48 (1993) 18178.
[40] L. Yang, Y. Liu, Q. Wang, H. Shi, G. Li, L. Zhang, Microelectron. Eng. 66 (2003) 192.
[41] S. Padovani, C. Sada, P. Mazzoldi, B. Brunetti, I. Borgia, A. Sgamellotti, A. Giulivi, F. D'Acapito, G. Battaglin, J. Appl. Phys. 93 (2003) 10058.
[42] G. Suyal, M. Mennig, H. Schmidt, J. Mater. Sci. 38 (2003) 1645.
[43] P. Mulvaney, Langmuir 12 (1996) 788.
[44] O. Bobin, M. Schvoerer, J.L. Miane, J.F. Fabre, J. Non-Cryst. Solids 332 (2003) 28.
[45] I. Borgia, B. Brunetti, I. Mariani, A. Sgamellotti, F. Cariati, P. Fermo, M. Mellini, C. Viti, G. Padeletti, Appl. Surf. Sci. 185 (2002) 206.
[46] Y.-C. Liu, H.-T. Lee, H.-H. Peng, Chem. Phys. Lett. 400 (2004) 436.
[47] R. Gupta, M.J. Dyer, W.A. Weimer, J. Appl. Phys. 92 (2002) 5264.
[48] G.C. Bond, D.T. Thompson, Catal. Rev. Sci. Eng. 41 (1999) 319.
[49] J. Miszei, P. Sipilä, V. Lantto, Sens. Actuators B 47 (1998) 139.

[50] U. Kreibig, M. Vollmer, Optical Properties of Metal Clusters, Springer-Verlag, Berlin, 1995.
[51] B. Wiley, Y. Sun, J. Chen, H. Cang, Z.-Y. Li, X. Li, Y. Xia, Mater. Res. Soc. Bull. 30 (2005) 356.
[52] E. Hutter, J.H. Fendler, Adv. Mater. 16 (2004) 1685.
[53] D. Barreca, A. Gasparotto, E. Tondello, G. Bruno, M. Losurdo, J. Appl. Phys. 96 (2004) 1655.
[54] V.E. Henrich, P.A. Cox, The Surface Science of Metal Oxides, Cambridge University Press, Cambridge, UK, 1994.
[55] F. Gonella, Nucl. Instrum. Methods Phys. Res., Sect. B 166 (2000) 831, and references therein.
[56] G. De Marchi, G. Mattei, P. Mazzoldi, C. Sada, A. Miotello, J. Appl. Phys. 92 (2002) 4249.
[57] G. De, A. Licciulli, C. Massaro, L. Tapfer, M. Catalano, G. Battaglin, C. Meneghini, P. Mazzoldi, J. Non-Cryst. Solids 194 (1996) 225.
[58] G. Schmid, J. Mater. Chem. 12 (2002) 1231.
[59] Z. Pászti, G. Petö, Z.E. Horváth, A. Karacs, L. Guczi, Solid State Commun. 107 (1998) 329.
[60] R. Chandra, P. Taneja, J. John, P. Ajjub, G.K. Dey, S.K. Kulshreshtha, Nanostruct. Mater. 11 (1999) 1171.
[61] M.A. van Huis, A.V. Fedorov, A. van Veen, C.V. Falub, S.W.H. Eijt, B.J. Kooi, J.Th.M. De Hosson, T. Hibma, R.L. Zimmerman, Nucl. Instrum. Methods Phys. Res., Sect. B 191 (2002) 442.
[62] U.K. Barik, S. Srinivasan, C.L. Nagendra, A. Subrahmanyam, Thin Solid Films 429 (2003) 129.
[63] C. Charton, M. Fahland, Vacuum 68 (2003) 65.
[64] W.-S. Ju, M. Matsuoka, K. Iino, H. Yamashita, M. Anpo, J. Phys. Chem. B 108 (2004) 2128.
[65] S. Scirè, S. Minicò, C. Crisafulli, S. Galvagno, Catal. Commun. 2 (2001) 229.
[66] N. Bogdanchikova, F.C. Meunier, M. Avalos-Borja, J.P. Breen, A. Pestryakov, Appl. Catal. B 36 (2002) 287.
[67] M.B. Cortie, E. van der Lingen, Mater. Forum 26 (2002) 1.
[68] D.W. Goodman, in: J.A. Schwarz, C.I. Contescu, K. Putyera (Eds.), Dekker Encyclopedia of Nanoscience and Nanotechnology, Taylor & Francis group, LLC, 2004, p. 611.
[69] Y. Xiong, H. Wu, Y. Guo, Y. Sun, D. Yang, D. Da, Thin Solid Films 375 (2000) 300.
[70] M. Okumura, S. Nakamura, S. Tsubota, T. Nakamura, M. Azuma, M. Haruta, Catal. Lett. 51 (1998) 53.
[71] E. Borsella, E. Cattaruzza, G. De Marchi, F. Gonella, G. Mattei, P. Mazzoldi, A. Quaranta, G. Battaglin, R. Polloni, J. Non-Cryst. Solids 245 (1999) 122.
[72] T. Suzuki, Y. Abe, M. Kawamura, K. Sasaki, T. Shouzu, K. Kawamata, Vacuum 66 (2002) 501.
[73] Y. Sarov, M. Nikolaeva, M. Sendova-Vassileva, D. Malinovska, J.C. Pivin, Vacuum 69 (2003) 321.
[74] H.B. Liao, R.F. Xiao, J.S. Fu, P. Yu, G.K.L. Wong, P. Sheng, Appl. Phys. Lett. 70 (1997) 1.
[75] I. Tanahashi, M. Yoshida, Y. Manabe, T. Tohda, Surf. Rev. Lett. 3 (1996) 1071.
[76] E. Cattaruzza, Nucl. Instrum. Methods Phys. Res., Sect. B 169 (2000) 141, and references therein.
[77] S. Deki, Y. Aoi, H. Yanagimoto, K. Ishii, K. Akamatsu, M. Mizuhata, A. Kajinami, J. Mater. Chem. 6 (1996) 1879, and references therein.
[78] H. Shinojima, J. Yumoto, S. Uesugi, Appl. Phys. Lett. 60 (1992) 298.
[79] X. Quélin, J. Sakars, A. Bourdon, P. Gadenne, Physica B 279 (2000) 102.
[80] M.A. El-Sayed, Acc. Chem. Res. 34 (2001) 257.
[81] F. Gonella, P. Mazzoldi, Metal nanocluster composite glasses, in: H.S. Nalwa (Ed.), Handbook of Nanostructured Materials and Nanotechnology, vol. 4, Academic Press, San Diego, 2000.
[82] G. Mattei, G. Battaglin, V. Bello, G. De Marchi, C. Maurizio, P. Mazzoldi, M. Parolin, C. Sada, J. Non-Cryst. Solids 322 (2003) 17.
[83] S. Padovani, F. D'Acapito, E. Cattaruzza, A. De Lorenzi, F. Gonella, G. Mattei, C. Maurizio, P. Mazzoldi, M. Montagna, S. Ronchin, C. Tosello, M. Ferrari, Eur. Phys. J. B 25 (2002) 11.
[84] L. Rivas, S. Sanchez-Cortes, J.V. García-Ramos, G. Morcillo, Langmuir 16 (2000) 9722.
[85] N.R. Jana, L.G. Gearheart, C.J. Murphy, Chem. Mater. 13 (2001) 2313.
[86] T. Ishizaka, S. Muto, Y. Kurokawa, Opt. Commun. 190 (2001) 385.
[87] R. Radnik, C. Mohr, P. Claus, Phys. Chem. Chem. Phys. 5 (2003) 172.
[88] Y. Iizuka, H. Fujiki, N. Yamuachi, T. Chijiiwa, S. Arai, S. Tsubota, M. Haruta, Catal. Today 36 (1997) 115.
[89] C.-y. Wang, C.-y. Liu, J. Chen, T. Shen, J. Colloid Interface Sci. 191 (1997) 464.
[90] K. Okazaki, Y. Morikawa, S. Tanaka, S. Ichikawa, K. Tanaka, M. Kohyama, Mater. Res. Soc. Symp. Proc. 738 (2003) G13.7.1.
[91] H. Sakurai, A. Ueda, T. Kobayashi, M. Haruta, Chem. Commun. (1997) 271.
[92] L. Zhang, F. Cosandey, R. Persuad, T.E. Madey, Surf. Sci. 439 (1999) 73.
[93] T. Ung, L.M. Liz-Marzán, P. Mulvaney, J. Phys. Chem. B 105 (2001) 3441.
[94] N. Pinçon, B. Palpant, D. Prot, E. Charron, S. Debrus, Eur. Phys. J. D 19 (2002) 395.
[95] S. Debrus, J. Lafait, M. May, N. Pinçon, D. Prot, C. Sella, J. Venturini, J. Appl. Phys. 88 (2000) 4469.
[96] N. Pinçon-Roetzinger, D. Prot, B. Palpant, E. Charron, S. Debrus, Mater. Sci. Eng. C 19 (2002) 51.
[97] J.F. Pérez-Robles, F.J. García-Rodríguez, J.M. Yáñez-Limón, F.J. Espinoza-Beltrán, Y.V. Vorobiev, J. González-Hernández, J. Phys. Chem. Solids 60 (1999) 1729.
[98] E. Cattaruzza, G. Battaglin, P. Calvelli, F. Gonella, G. Mattei, C. Maurizio, P. Mazzoldi, S. Padovani, R. Polloni, C. Sada, B.F. Scremin, F. D'Acapito, Compos. Sci. Technol. 63 (2003) 1203.
[99] D. Manikandan, S. Mohan, K.G.M. Nair, Mater. Lett. 58 (2004) 907.
[100] K. Uchida, S. Kaneko, S. Omi, C. Hata, H. Tanji, Y. Asahara, A.J. Ikushima, T. Tokizaki, A. Nakamura, J. Opt. Soc. Am. B: Opt. Phys. 11 (1994) 1236.
[101] I. Tanahashi, Y. Manabe, T. Tohda, S. Sasaki, A. Nakamura, J. Appl. Phys. 79 (1996) 1244.
[102] H.B. Liao, W.J. Wen, G.K.L. Wong, J. Appl. Phys. 93 (2003) 4485.
[103] S. Dhara, R. Kesavamoorthy, P. Magudapathy, M. Premila, B.K. Panigrahi, K.G.M. Nair, C.T. Wu, K.H. Chen, L.C. Chen, Chem. Phys. Lett. 370 (2003) 254.
[104] F. Hache, D. Ricard, C. Flytzanis, J. Opt. Soc. Am. B: Opt. Phys. 3 (1986) 1647.
[105] O. Maruyama, Y. Senda, S. Omi, J. Non-Cryst. Solids 259 (1999) 100.
[106] P. Mazzoldi, G.W. Arnold, G. Battaglin, F. Gonella, R.F. Haglund Jr., J. Nonlin. Opt. Phys. Mater. 5 (1996) 285.
[107] A. Hagfeldt, M. Grätzel, Acc. Chem. Res. 33 (2000) 269.
[108] S.M. Prokes, W.E. Carlos, J.L. Gole, C. She, T. Lian, Mater. Res. Soc. Symp. Proc. 738 (2003) G8.9.1.
[109] N. Chandrasekharan, P.V. Kamat, J. Phys. Chem. B 104 (2000) 10851.
[110] N.J. Cherepy, G.P. Smestad, M. Grätzel, J.Z. Zhang, J. Phys. Chem. B 101 (1997) 9342.
[111] L. Armelao, D. Barreca, G. Bottaro, A. Gasparotto, E. Tondello, M. Ferroni, S. Polizzi, Chem. Mater. 16 (2004) 3331.
[112] L. Armelao, D. Barreca, G. Bottaro, A. Bovo, A. Gasparotto, E. Tondello, Surf. Sci. Spectra 10 (2003) 1.
[113] D. Barreca, A. Gasparotto, C. Maragno, E. Tondello, S. Gialanella, J. Appl. Phys. 97 (2005) 54311.
[114] L. Armelao, D. Barreca, G. Bottaro, A. Gasparotto, C. Maragno, E. Tondello, Surf. Sci. Spectra 10 (2003) 170.
[115] D. Barreca, A. Bovo, A. Gasparotto, E. Tondello, Surf. Sci. Spectra 10 (2003) 21.
[116] L. Armelao, D. Barreca, A. Gasparotto, E. Pierangelo, E. Tondello, S. Polizzi, J. Nanosci. Nanotechnol. 5 (2005) 259.
[117] L. Armelao, D. Barreca, G. Bottaro, G. Mattei, C. Sada, E. Tondello, Chem. Mater. 17 (2005) 1450.
[118] L. Armelao, R. Bertoncello, M. De Dominicis, Adv. Mater. 9 (1997) 736.
[119] C.N.R. Rao, A. Müller, A.K. Cheetham, The Chemistry of Nanomaterials, Wiley-VCH, Weinheim, 2004.

[120] J. Hu, T.W. Odom, C.M. Lieber, Acc. Chem. Res. 32 (1999) 435.
[121] Y. Xia, P. Yang, Y. Sun, Y. Wu, B. Mayers, B. Gates, Y. Yin, F. Kim, H. Yan, Adv. Mater. 15 (2003) 353.
[122] C. Ji, P.C. Searson, J. Phys. Chem. B 107 (2003) 4494.
[123] J. Pérez-Juste, I. Pastoriza-Santos, L.M. Liz-Marzan, P. Mulvaney, Coord. Chem. Rev. 249 (2005) 1870.
[124] Y. Sun, Y. Xia, Science 298 (2002) 2176.
[125] S.-S. Chang, C.-W. Shih, C.-D. Chen, W.-C. Lai, C.R.C. Wang, Langmuir 15 (1999) 701.
[126] A.J. Haes, D.A. Stuart, S. Nie, R.P. Van Duyne, J. Fluoresc. 14 (2004) 355.
[127] M. Geissler, H. Wolf, R. Stutz, E. Delamarche, U.-W. Grummt, B. Michel, A. Bietsch, Langmuir 19 (2003) 6301.
[128] Q. Zhang, Y. Li, D. Xu, Z. Gu, J. Mater. Sci. Lett. 20 (2001) 925.
[129] C.R. Martin, Science 266 (1994) 1961.
[130] R. Zhu, Y.T. Pang, Y.S. Feng, G.H. Fu, Y. Li, L.D. Zhang, Chem. Phys. Lett. 368 (2000) 696.
[131] R.M. Dickinson, L.A. Lyon, J. Phys. Chem. B 104 (2000) 6095.
[132] A. Cabañas, D.P. Long, J.J. Watkins, Chem. Mater. 16 (2004) 2028.
[133] C.N.R. Rao, J. Mater. Chem. 9 (1999) 1.
[134] A.P. Alivisatos, P.F. Barbara, A.W. Castleman, J. Chang, D.A. Dixon, M.L. Klein, G.L. McLendon, J.S. Miller, M.A. Ratner, P.J. Rossky, S.I. Stupp, M.E. Thompson, Adv. Mater. 10 (1997) 1297.
[135] K. Murakoshi, H. Tanaka, Y. Sawai, Y. Nakato, Surf. Sci. 532–535 (2003) 1109.
[136] J. Sharma, N.K. Chaki, A.B. Mandale, R. Pasricha, K. Vijayamohanan, J. Colloid Interface Sci. 272 (2004) 145.
[137] E. Feurer, H. Suhr, Appl. Phys. A 44 (1987) 171.
[138] Y. Kobayashi, M.A. Correa-Duarte, L.M. Liz-Marzán, Langmuir 17 (2001) 6375.
[139] A. Dutta, D. Das, M.L. Grilli, E. Di Bartolomeo, E. Traversa, D. Chakravorty, J. Sol–Gel Sci. Technol. 26 (2003) 1085.
[140] P.I. Paulose, G. Jose, V. Thomas, G. Jose, N.V. Unnikrishnan, M.K.R. Warrier, Bull. Mater. Sci. 25 (2002) 69.
[141] J.L. Mohanan, S.L. Brock, Chem. Mater. 15 (2003) 2567.
[142] D. Das, D. Chakravorty, Appl. Phys. Lett. 76 (2000) 1273.
[143] V.S. Gurin, A.A. Alexeenko, K.V. Yumashev, R. Prokoshin, S.A. Zolotovskaya, G.A. Zhavnerko, Mater. Sci. Eng. C 23 (2003) 1063.
[144] J. Manzanares-Martínez, L.A. García-Cerda, R. Ramírez-Bon, F.J. Espinoza-Beltrán, J.F. Pérez-Robles, J. González-Hernández, Thin Solid Films 365 (2000) 30.
[145] T. Lutz, C. Estourès, J.C. Merle, J.L. Guille, J. Alloys Compd. 262 (1997) 438.
[146] M. Nogami, Y. Abe, A. Nakamura, J. Mater. Res. 10 (1995) 2648.
[147] F. Pérez-Robles, F.J. García-Rodríguez, S. Jiménez-Sandoval, J. González-Hernández, J. Raman Spectrosc. 30 (1999) 1099.
[148] N. Maruse, K. Kuraoka, T. Yazawa, Mol. Cryst. Liq. Cryst. 314 (1998) 273.
[149] E.M.B. de Sousa, A.P. Guimaraes, N.D.S. Mohallem, R.M. Lago, Appl. Surf. Sci. 183 (2001) 216.
[150] A. Mendoza-Galván, J.F. Pérez-Robles, F.J. Espinoza-Beltrán, R. Ramirez-Bon, Y.V. Vorobiev, J. González-Hernández, G. Martinez, J. Vac. Sci. Technol. A 17 (1999) 1103.
[151] G. Cordoba, R. Arroyo, J.L.G. Fierro, M. Viniegra, J. Solid State Chem. 123 (1996) 93.
[152] M. Lee, L. Chae, K.C. Lee, Nanostruct. Mater. 11 (1999) 195.
[153] M. Epifani, C. Giannini, L. Tapfer, L. Vasanelli, J. Am. Ceram. Soc. 83 (2000) 2385.
[154] H. Shi, L. Zhang, W. Cai, Mater. Res. Bull. 35 (2000) 1689.
[155] Y. Zhou, C.H. Ma, H. Itoh, K. Naka, Y. Chujo, Chem. Lett. 12 (2002) 1170.
[156] W. Chen, J.Y. Zhang, Y. Di, I.W. Boyd, Inorg. Chem. Commun. 6 (2003) 950.
[157] G. Fu, W. Cai, C. Kan, C. Li, L. Zhang, Appl. Phys. Lett. 83 (2003) 36.
[158] W. Chuanyi, L. Chunyan, S. Tao, Chin. Sci. Bull. 43 (1998) 210.
[159] G. Battaglin, E. Cattaruzza, F. Gonella, R. Polloni, F. D'Acapito, S. Colonna, G. Mattei, C. Maurizio, P. Mazzoldi, S. Padovani, C. Sada, A. Quaranta, A. Longo, Nucl. Instrum. Methods Phys. Res., Sect. B 200 (2003) 185, and references therein.
[160] E. Borsella, G. De Marchi, F. Caccavale, F. Gonella, G. Mattei, P. Mazzoldi, G. Battaglin, A. Quaranta, A. Miotello, J. Non-Cryst. Solids 253 (1999) 261.
[161] G.H. Takaoka, T. Hamano, K. Fukushima, J. Matsuo, I. Yamada, Nucl. Instrum. Methods Phys. Res., Sect. B 121 (1997) 503.
[162] S. Schiestel, C.M. Cotell, C.A. Carosella, K.S. Grabowski, G.K. Hubler, Nucl. Instrum. Methods Phys. Res., Sect. B 127–128 (1997) 566.
[163] A.L. Stepanov, D.E. Hole, P.D. Townsend, Nucl. Instrum. Methods Phys. Res., Sect. B 166–167 (2000) 882.
[164] H. Tsuji, K. Kurita, Y. Gotoh, N. Kishimoto, J. Ishikawa, Nucl. Instrum. Methods Phys. Res., Sect. B 195 (2002) 315.
[165] K. Fukumi, A. Chayahara, K. Kadono, T. Sakaguchi, Y. Horino, M. Miya, K. Fujii, J. Hayakawa, J. Appl. Phys. 75 (1994) 3075.
[166] M. Ferrari, L.M. Gratton, A. Maddalena, M. Montagna, C. Tosello, J. Non-Cryst. Solids 191 (1995) 101.
[167] K. Luo, D.Y. Kim, D.W. Goodman, J. Mol. Catal. A: Chem. 167 (2001) 191.
[168] M. Adamik, P.B. Barna, I. Tomov, Thin Solid Films 359 (2000) 33.
[169] H.C. Kim, T.L. Alford, D.R. Allee, Appl. Phys. Lett. 81 (2002) 8287.
[170] Q. Guo, K. Luo, K.A. Davis, D.W. Goodman, Surf. Interface Anal. 32 (2001) 161.
[171] S.C. Parker, A.W. Grant, W.A. Bondzie, C.T. Campbell, Surf. Sci. 441 (1999) 10.
[172] T. Sasaki, N. Koshizaki, M. Koinuma, Y. Matsumoto, Nanostruct. Mater. 12 (1999) 511.
[173] J.-W. Yoon, T. Sasaki, M. Koshizaki, E. Traversa, Scripta Mater. 44 (2001) 1865.
[174] H. Ishikawa, T. Ida, K. Kimura, Surf. Rev. Lett. 3 (1996) 1153.
[175] A. Rizzo, M.A. Tagliente, M. Alvisi, S. Scaglione, Thin Solid Films 396 (2001) 29.
[176] S. Terauchi, N. Koshizaki, H. Umehara, Nanostruct. Mater. 5 (1995) 71.
[177] J. Mizsei, P. Sipilä, V. Lantto, Sens. Actuators B 47 (1998) 139.
[178] F. Parmigiani, M. Scagliotti, G. Samoggia, G.P. Ferraris, Thin Solid Films 125 (1985) 229.
[179] S. Lee, J. Hong, S.-g. Oh, Surf. Coat. Technol. 94–95 (1997) 368.
[180] D.A. Glocker, S.I. Shah, Handbook of Thin Film Process Technology, Institute of Physics Publishing, Bristol, UK, 1995.
[181] D. Dalacu, L. Martinu, J. Appl. Phys. 87 (2000) 228.
[182] C.J. Brinker, G.W. Scherer, Sol–Gel Science: The Physics and Chemistry of Sol–Gel Processing, Academic Press, New York, 1990.
[183] L.L. Hench, J.K. West, Chem. Rev. 90 (1990) 33.
[184] U. Schubert, N. Hüsing, Synthesis of Inorganic Materials, Wiley, VCH, 2000.
[185] S. Sakka, H. Kozuka, J. Sol–Gel Sci. Technol. 13 (1998) 701.
[186] B. Breitscheidel, J. Zieder, U. Schubert, Chem. Mater. 3 (1991) 559.
[187] M. Catalano, E. Carlino, G. De, L. Tapfer, F. Gonella, P. Mazzoldi, G. Battaglin, Philos. Mag. B 76 (1997) 621.
[188] G. De, J. Sol–Gel Sci. Technol. 11 (1998) 289.
[189] H. Schmidt, G. Jonschker, S. Goedicke, M. Mennig, J. Sol–Gel Sci. Technol. 19 (2000) 39.
[190] U. Schubert, Adv. Eng. Mater. 6 (2004) 173.
[191] J.D. Mackenzie, J. Sol–Gel Sci. Technol. 1 (1993) 7.
[192] W. Rupp, N. Hüsing, U. Schubert, J. Mater. Chem. 12 (2002) 2594.
[193] M. Catalano, E. Carlino, M.A. Tagliente, A. Licciulli, L. Tapfer, Microsc. Microanal. Microstruct. 6 (1995) 611.
[194] K.M. Choi, K.J. Shea, J. Am. Chem. Soc. 116 (1994) 9052.
[195] G.J. de A.A. Soler-Illia, C. Sanchez, B. Lebeau, J. Patarin Chem. Rev. 102 (2002) 4093.
[196] U. Schubert, J. Chem. Soc., Dalton Trans. (1996) 3343.
[197] J. Brinker, J. Non-Cryst. Solids 100 (1988) 31.
[198] W. Morke, R. Lamber, U. Schubert, B. Breitscheidel, Chem. Mater. 6 (1994) 1659.
[199] S. Bharathi, O. Lev, Chem. Commun. 23 (1997) 2303.

[200] T. Gacoin, F. Chaput, J.P. Boilot, G. Jaskierowicz, Chem. Mater. 5 (1993) 1150.
[201] A. Martino, S.A. Yamanaka, J.S. Kawola, D.A. Loy, Chem. Mater. 9 (1997) 423.
[202] J.E. Mahan, Physical Vapor Deposition of Thin Films, J. Wiley & Sons, Chichester, UK, 2000.
[203] S. Cho, S. Lee, S.G. Oh, S.J. Park, W.M. Kim, B.K. Cheong, M. Chung, K.B. Song, T.S. Lee, S.G. Kim, Thin Solid Films 377 (2000) 97.
[204] L. Armelao, D. Barreca, L. Bigliani, G. Bottaro, A. Gasparotto, E. Tondello, Electrochem. Soc. Proc. 2003–08 (2003) 1119.
[205] L. Armelao, D. Barreca, G. Bottaro, A. Gasparotto, E. Tondello, M. Ferroni, S. Polizzi, Chem. Vap. Deposition 10 (2004) 257.
[206] L. Armelao, D. Barreca, G. Bottaro, A. Gasparotto, C. Maragno, E. Tondello, Chem. Mater. 17 (2005) 427.
[207] L. Armelao, D. Barreca, G. Bottaro, A. Gasparotto, C. Maragno, E. Tondello, C. Sada, J. Nanosci. Nanotechnol. 5 (2005) 781.
[208] L. Armelao, D. Barreca, G. Bottaro, A. Gasparotto, C. Maragno, E. Tondello, Surf. Sci. Spectra 10 (2003) 143.
[209] C. Renard, C. Ricolleau, E. Fort, S. Besson, T. Gacoin, J.-P. Boilot, Appl. Phys. Lett. 80 (2002) 300.
[210] F.F. Ferreira, P.S. Haddad, M.C.A. Fantini, G.E.S. Brito, Solid State Ionics 165 (2003) 161.
[211] K.M. Choi, K.J. Shea, J. Phys. Chem. 98 (1994) 3207.
[212] L. Armelao, S. Gross, E. Cattaruzza, R. Bertoncello, G. Mattei, S. Gialanella, P. Mazzoldi, E. Tondello, J. Mater. Chem. 12 (2002) 2401.
[213] L. Armelao, D. Barreca, M. Bertapelle, G. Bottaro, C. Sada, E. Tondello, Mater. Res. Soc. Symp. Proc. 737 (2003) F8.27.1.
[214] G. Battaglin, E. Cattaruzza, F. Gonella, R. Polloni, B.F. Scremin, G. Mattei, P. Mazzoldi, C. Sada, Appl. Surf. Sci. 226 (2004) 52.
[215] K. Borgohain, J.B. Singh, M.V. Rama Rao, T. Shripathi, S. Mahamuni, Phys. Rev. B 61 (2000) 11093.
[216] M.A. Brookshier, C.C. Chusuei, D.W. Goodman, Langmuir 15 (1999) 2043.
[217] B. Balamurugan, B.R. Mehta, S.M. Shivaprasad, Appl. Phys. Lett. 79 (2001) 3176.
[218] V.R. Palkar, A. Pushan, S. Chattopadhyay, M. Multani, Phys. Rev. B 53 (1996) 2167.
[219] M. Mennig, J. Spanhel, H. Schmidt, S. Betzholz, J. Non-Cryst. Solids 147–148 (1992) 326.
[220] A. Henglein, T. Linnert, P. Mulvaney, Phys. Chem. 94 (1990) 1449.
[221] J.M. Moulder, W.F. Stickle, P.E. Sobol, K.D. Bomben, Handbook of X-Ray Photoelectron Spectroscopy, Perkin-Elmer, Eden Prairie, MN, 1992.
[222] L. Armelao, D. Barreca, G. Bottaro, S. Gross, A. Gasparotto, C. Maragno, E. Tondello, A. Zattin, Surf. Sci. Spectra 10 (2003) 137.
[223] D. Briggs, M.P. Seah, Practical Surface Analysis, vol. 1, Auger and X-Ray Photoelectron Spectroscopy, J. Wiley & Sons, New York, 1990.
[224] C.D. Wagner, L.H. Gale, R.H. Raymond, Anal. Chem. 51 (1979) 466.
[225] D.V. Ragone, Thermodynamics of Materials, Wiley, New York, 1995.
[226] J.A. Rodriguez, J.Y. Kim, J.C. Hanson, M. Pérez, A.I. Frenkel, Catal. Lett. 85 (2003) 247.
[227] A. Grill, Cold Plasma in Materials Fabrication, IEEE Press, New York, USA, 1993.
[228] Y. Catherine, Diamond and diamond-like films and coatings, in: R.E. Clausing, L.L. Horton, J.C. Angus, P. Koidl (Eds.), NATO-ASI Series B: Physics, vol. 266, Plenum Press, New York, 1991, p. 193.
[229] G.H. Tompkins, A.W. McGahan, Spectroscopic Ellipsometry and Reflectometry, J. Wiley & Sons, New York, 1999.
[230] M. Losurdo, A. Grimaldi, M. Giangregorio, P. Capezzuto, G. Bruno, J. Phys. IV 11 (2001) Pr3-1175.
[231] B.P. Zhang, H. Masumoto, Y. Romeno, T. Goto, Mater. Trans., JIM 43 (2002) 2855.
[232] F. Parmigiani, G. Samoggia, G.P. Ferraris, J. Appl. Phys. 57 (1985) 2524.
[233] A. Maekawa, F. Okuyama, Surf. Sci. 481 (2001) L427.
[234] K. Okada, N. Yamamoto, Y. Kameshima, A. Yasumori, K.J.D. MacKenzie, J. Am. Ceram. Soc. 84 (2001) 1591.
[235] Md. Mosaddeq-ur-Rahman, G. Yu, K.M. Krishna, T. Soga, J. Watanabe, T. Jimbo, M. Umeno, Appl. Opt. 37 (1998) 691.
[236] D. Barreca, A. Gasparotto, E. Tondello, J. Nanosci. Nanotechnol. 5 (2005) 994, and references therein.
[237] M.L. Steen, W.C. Flory, N.E. Capps, E.R. Fisher, Chem. Mater. 13 (2001) 2749.
[238] Y.-J. Han, J.M. Kim, G.D. Stucky, Chem. Mater. 12 (2000) 2068.
[239] S. Yu, N. Li, J. Wharton, C.R. Martin, Nano Lett. 3 (2003) 815.
[240] W.-B. Zhao, J.-J. Zhu, H.-Y. Chen, J. Cryst. Growth 258 (2003) 176.
[241] Z. Wang, H.L. Li, Appl. Phys. A 74 (2002) 201.
[242] C.A. Foss Jr., G.L. Hornyak, J.A. Stockert, C.R. Martin, J. Phys. Chem. 98 (1994) 2963.